ELECTROMAGNETIC ANALYSIS AND DESIGN OF MINIATURIZED BRANCHLINE COUPLERS

A THESIS SUBMITTED TO
THE GRADUATE SCHOOL OF NATURAL AND APPLIED SCIENCE
OF
MIDDLE EAST TECHNICAL UNIVERSITY

BY

GALİP ORKUN ARICAN

IN PARTIAL FULLFILLMENT OF THE REQUIREMENTS
FOR
THE DEGREE OF MASTER OF SCIENCE
IN
ELECTRICAL AND ELECTRONICS ENGINEERING

JULY 2014

Approval of the thesis:

ELECTROMAGNETIC ANALYSIS AND DESIGN OF MINIATURIZED BRANCHLINE COUPLERS

submitted by **GALİP ORKUN ARICAN** in partial fulfillment of the requirements for the degree of Master of Science in **Electrical and Electronics Engineering Department, Middle East Technical University** by,

Prof. Dr. Canan ÖZGEN
Dean, Graduate School of **Natural and Applied Science**

Prof. Dr. Gönül TURHAN SAYAN
Head of Department, **Electrical and Electronics Engineering**

Prof. Dr. Gönül TURHAN SAYAN
Supervisor, **Electrical and Electronics Engineering Dept., METU**

Dr. Özlem ŞEN
Co-Supervisor, **NANOTAM, Bilkent University**

Examining Committee Members:

Prof. Dr. Canan TOKER
Electrical and Electronics Engineering Dept., METU

Prof. Dr. Gönül TURHAN SAYAN
Electrical and Electronics Engineering Dept., METU

Prof. Dr. Ekmel ÖZBAY
Electrical and Electronics Engineering Dept., Bilkent University

Dr. Fatih KOÇER
Electrical and Electronics Engineering Dept., METU

Dr. Özlem ŞEN
Researcher, NATOTAM, Bilkent University

Date: 10.07.2014

I hereby declare that all information in this document has been obtained and presented in accordance with academic rules and ethical conduct. I also declare that, as required by these rules and conduct, I have fully cited and referenced all material and results that are not original to this work.

Name, Last name: Galip Orkun ARICAN

Signature :

ABSTRACT

ELECTROMAGNETIC ANALYSIS AND DESIGN OF MINIATURIZED BRANCHLINE COUPLERS

Arıcan, Galip Orkun
M.S., Department of Electrical and Electronics Engineering
Supervisor: Prof. Dr. Gönül Turhan Sayan
Co-Supervisor: Dr. Özlem Şen

July 2014, 89 pages

Branchline couplers are widely used components in the design of microwave devices. In addition to other applications, these couplers have been crucial elements for high power GaN based MMIC designs where layout space limitations are known to be critical. The conventional branchline couplers designed by four quarter wavelenght transmission lines. This type of conventional branchline coupler covers a large physical area that leads to high costs in MMIC fabrication. Therefore, design of miniaturized branchline coupler with increased operational bandwidth is important to minimize the chip size and increase the bandwidth of system. In additional, usage of optimum electromagnetic simulation in terms of accuracy and simulation time is significant to reduce the simulation time without suffering from the loss of accuracy. In this thesis, branchline couplers will be analyzed and designed paying special attention to increase the operation bandwidth and reduce the area as small as possible. Different electromagnetic solvers will be used to analyze the coupler topologies and results will be compared in terms of accuracy and simulation time.

Keywords: Branchline Coupler, Coplanar Waveguide (CPW), miniaturization

ÖZ

MİNYATÜRLEŞTİRİLMİŞ DAL-HAT KUPLÖRLERİNİN ELEKTROMANYETİK ANALİZİ VE TASARIMI

Arıcan, Galip Orkun
Yüksek Lisans, Elektrik Elektronik Mühendisliği Bölümü
Tez Yürütücüsü: Prof. Dr. Gönül Turhan Sayan
Ortak Tez Yürütücüsü: Dr. Özlem Şen

Temmuz 2014, 89 sayfa

Dal-hat kuplörleri mikrodalga gereçlerinin tasarımında yaygın bir şekilde kullanılırlar. Diğer uygulamalarının yanısıra, bu kuplörler serimdeki yer kısıtlamalarının kritik olduğu bilinen yüksek güçlü GaN tabanlı MMIC tasarımlarında da kullanılan çok önemli elemanlardır. Klasik dal-hat kuplörler çeyrek dalga boyunda dört hat kullanılarak tasarlanmaktadır ve bunun neticesinde bu tür klasik dal-hat kuplörler büyük alanlar kaplamakta olup MMIC üretim maliyetleri artmaktadır. Geniş çalışma frekans aralığı sahip minyatürleştirilmiş dal-hat kuplörler yonca boyutlarının düşürülmesi ve sistem bant genişliğinin artırılması için önemlidir. Bununla beraber, elektromanyetik simülasyonların doğruluk ve zaman konularında en uygun şekilde kullanılması simülasyon doğruluğunda azalma olmadan simulasyon süresinin kısaltması açısından önem taşımaktadır. Bu tezde, dal-hat kuplörlerin analizi ve tasarımı gerçekleştirilirken, çalışma frekans genişliğinin artırılmasına ve boyutların olabildiğince küçültülmesine özel önem verilecektir ve farklı elektromanyetik simülatörler kullanılarak simülasyon sonuçları doğruluk ve süre konularında karşılaştırılacaktır.

Anahtar kelimeler: Dal-hat kuplör, Eş düzlemli dalga kılavuzu (CPW), minyatürleştirme

To my beloved family

ACKNOWLEDGEMENT

I would like to express my gratitude to my supervisor Prof. Dr. Gönül Turhan Sayan and my co-advisor Dr. Özlem Şen, for their support and invaluable comments in my thesis work.

I am also grateful to Prof. Dr. Ekmel Özbay, for his continuous support and encouragement. It is an honor for me to take part in various advanced projects with Nanotam members. Also, special thanks to Ömer Cengiz for his generous help.

I am thankful to Özge Baydar for her unconditional support and encouragements during my thesis work.

Finally, my special thanks belong to my lovely family for their encouragement, understanding and unconditional love. I hereby dedicate my thesis work to my parents, Firdevs Arıcan and Yücel Arıcan and to my brother, Dr. Gökhun Arıcan.

TABLE OF CONTENTS

ABSTRACT v

ÖZ vi

ACKNOWLEDGEMENT ix

TABLE OF CONTENTS x

LIST OF TABLES xiii

LIST OF FIGURES xiv

LIST OF ABBREVIATIONS xvii

CHAPTERS

1. INTRODUCTION 1

2. DIRECTIONAL COUPLER 5

2.1 Overview of Microwave Couplers 5

2.2 Basics of Directional Coupler 7

2.2.1 S-Parameters Analysis of Directional Couplers 9

2.3 Hybrid Couplers 12

2.3.1 90˚ Hybrid Couplers (3dB) 13

2.3.2 180˚ Hybrid Couplers (3dB) 14

3. SYNTHESIS OF MINIATURIZED BRANCHLINE COUPLERS 17

3.1 The Conventional Branchline Hybrid Coupler 18

3.2 Theoretical Analysis of the Branchline Coupler 19

3.2.1 Properties of BLC 29

3.3 New Design Approach 29

3.3.1 Lumped Element Technique 30
3.3.2 T-shape Structures 30
3.3.3 π-shape Structures 33
3.3.4 Meandering the Transmission Lines 35
4. MINIATURIZED BRANCHLINE COUPLER DESIGN FOR X-BAND APPLICATIONS 37
4.1 General Design Considerations of the Miniaturized Branchline Coupler 38
4.1.1 mBLC Design with Using ADS CPW Tools 39
4.2 Design of the Miniaturized Branchline Coupler in ADS Momentum 44
4.2.1 The first mBLC Design in ADS Momentum 47
4.2.2 The second mBLC Design in ADS Momentum 48
4.3 Simulation Results of the mBLC Designs in ADS Momentum 49
4.3.1. Simulation Results of first mBLC Design in ADS Momentum 52
4.3.2 Simulation Results of second mBLC Design in ADS Momentum 53
4.4 Design of the Miniaturized Branchline Couplers in Sonnet Suites 55
4.5 Simulation Results of the mBLC Designs in Sonnet Suites 63
4.5.1 Simulation Results of the first mBLC Designs in Sonnet Suites 63
4.5.1 Simulation Results of the first mBLC Designs in Sonnet Suites 65
4.6 Photomask Design 67
5. MEASUREMENT RESULTS 69
5.1 S-Parameter Measurements 69
5.1.1 S-Parameter Measurement Results of mBLC for the First Design 72
5.1.2 S-Parameter Measurement Results of mBLC for the Second Design 74
5.2 The Comparison of EM Simulation Results with Measurement Results 75

5.2.1 The Comparison of EM Simulation Results with Measurement Results for the first mBLC design 76

5.2.2 The Comparison of EM Simulation Results with Measurement Results for the second mBLC design 79

6. CONCLUSION & FUTURE WORKS 83

REFERENCES 87

LIST OF TABLES

TABLES

Table 3.1: The incident and reflected voltage values of each port in branchline coupler [17]..... 23
Tablo 4.1: The Comparisons between Conventional BLC and mBLC designs.... 67
Table 5.1: The Comparison of EM Simulation Results with Measurement Results of the first mBLC design..... 78
Table 5. 2: The Comparison of EM Simulation Results with Measurement Results of the second mBLC design 81
Table 6.1: The Properties of Fabricated mBLCs 84

LIST OF FIGURES

FIGURES

Figure 2.1 a) Power Divider b) Power Combiner 5
Figure 2.2: Block Diagram of Directional Coupler 7
Figure 2.3: Block Diagram of Commercial Directional Coupler..... 8
Figure 2.4: Directional Coupler Mechanisms 8
Figure 2.5: 90˚ Hybrid Coupler (3dB) 13
Figure 2.6: 180˚ Hybrid Coupler (3dB) 14
Figure 3.1: The Conventional Branchline Coupler 18
Figure 3.2: The schematic of the branchline coupler 19
Figure 3.3: Even /Odd Mode Analysis of BLC..... 20
Figure 3.4: Even Mode Analysis of BLC 21
Figure 3.5: Odd Mode Analysis of BLC 21
Figure 3.6: Even Mode Analysis of BLC and Equivalent Circuit 22
Figure 3.7: Odd Mode Analysis of BLC and Equivalent Circuit..... 22
Figure 3.8: The General Equivalent Circuit of the Splitted BLC 25
Figure 3.9: a) λ/4 Transmission Line b) T-shaped Structure Equivalent to (a) 31
Figure 3.10: T-shaped Structure Circuit Representations 31
Figure 3.11: a) λ/4 Transmission Line b) π-shaped Structure Equivalent to (a)... 33
Figure 3.12: π-shaped Structure Circuit Representations 33
Figure 3.13: Meander Section 36
Figure 4.1: Schematic of the mBLC in ADS 40
Figure 4.2: Schematic of the mBLC with Meander Sections in ADS 41
Figure 4.3: Substrate Parameters..... 42
Figure 4.4: S-parameter Simulation Results of the mBLC with ideal CPW TLs in ADS 42

Figure 4.5: Direct (S21) and Coupled (S31) Port Transmission of the mBLC with ideal CPW TLs in ADS 43
Figure 4.6: Phase Difference Between the Output Ports of mBLC with ideal CPW TLs in ADS 43
Figure 4.7: Layer Definitions of ADS Momentum 45
Figure 4.8: Substrate Definition of ADS Momentum 46
Figure 4.9: Air Bridge Design in ADS Momentum 47
Figure 4.10: Layout and its 3-D view of the first mBLC in ADS Momentum 48
Figure 4.11: 2D Layout and its 3-D view in ADS Momentum for the second mBLC 49
Figure 4.12: Port Definitions of ADS Momentum 50
Figure 4.13: Mesh Property of ADS Momentum 51
Figure 4.14: Frequency Plan of ADS Momentum 51
Figure 4.15: EM Simulation Results (ADS Momentum) of mBLC for the first design a) Input/Output Reflections b) Through (S21) and Coupled (S31) Port Transmission c) Phase Difference between the Output Ports 52
Figure 4.16: Volume Current Density of the mBLC for the first design 53
Figure 4.17: EM Simulation Results (ADS Momentum) of mBLC for the second design a) Input/Output Reflections b) Through (S21) and Coupled (S31) Port Transmission c) Phase Difference between the output ports 54
Figure 4.18: The Volume Current Density of the mBLC for the second Design . 55
Figure 4.19: Dielectric Layers of the mBLC in the Sonnet Suites 56
Figure 4.20: Metal Types of the mBLC in the Sonnet Suites 57
Figure 4.21: Air Bridge and Underpass Structures in the Sonnet Suite 58
Figure 4.22: 2-D Layout and 3-D view of the mBLC for the first design in Sonnet Suites 59
Figure 4.23: 2-D Layout and 3-D view of the mBLC for the second design in Sonnet Suites 60
Figure 4.24: Ports of the mBLC in Sonnet Suites 61
Figure 4.25: Box Settings of the mBLC in Sonnet Suites 62
Figure 4.26: Analysis Settings of the mBLC in Sonnet Suites 62

Figure 4.27: EM Simulation Results (Sonnet) of mBLC for the first design 64
Figure 4.28: Current Density (Sonnet) of mBLC for the first design 64
Figure 4.29: EM Simulation Results (Sonnet) of mBLC for the second design... 65
Figure 4.30: Current Density (Sonnet) of mBLC for the second design 66
Figure 4.31: Photomask Design including mBLCs..... 68
Figure 5.1: Photography of S-parameter Measurement Setup 70
Figure 5.2: Photography of mBLC under test 71
Figure 5.3: Photography of the first mBLC design..... 72
Figure 5.4: S-parameter Measurement Results of the first mBLC design 73
Figure 5.5: Photography of the second mBLC design 74
Figure 5.6: S-parameter Measurement Results of the second mBLC design 75
Figure 5.7: S-parameter Simulation and Measurement Results a) S11 b) S22 c) S33 d) S21 and e) S31 of the first mBLC design (EM Simulation Results of ADS Momentum (Red), EM Simulation Results of Sonnet Suietes (Blue) and Measured Results (Purple)) 76
Figure 5.8: Phase Difference between the output ports of the first mBLC design in the frequency bandwidth of a) 7GHz - 10GHz b) 8GHz – 12 GHz (ADS Momentum (Red), Sonnet Suietes (Blue) and Measured Results (Purple)) .. 77
Figure 5.9: S-parameter Simulation and Measurement Results a) S11 b) S22 c) S33 d) S21 and e) S31 of the second mBLC design (EM Simulation Results of ADS Momentum (Red), EM Simulation Results of Sonnet Suietes (Blue) and Measured Results (Purple)) 79
Figure 5.10: Phase Difference between the output ports of the second mBLC design in the frequency bandwidth of a) 7GHz - 10GHz b) 8GHz - 13 GHz (ADS Momentum (Red), Sonnet Suietes (Blue) and Measured Results (Purple)) .. 80

LIST OF ABBREVIATIONS

ADS	Advanced Design System
BLC	Branchline Coupler
CPW	Coplanar Waveguide
EM	Electro-Magnetic
mBLC	Miniaturized Branchline Coupler
MMIC	Monolithic Microwave Integrated Circuit
MoM	Method of Moment
TL	Transmission Line

CHAPTER 1

INTRODUCTION

Branchline coupler is a special type of directional coupler which has become one of the most popular key components in microwave frequencies since the earliest directional coupler was invented in 1922 [1]. The features such as low cost, low losses and design simplicity have made the branchline coupler (BLC) a highly desirable component in radio frequency (RF) applications. Later on, with the enhancements in fabrication technologies mass production, the sizes of digital circuits designed for commercial and military applications have been decreased significantly while the size of microwave components have not been significantly reduced [2]. Therefore, it has been a challenge for engineers and researchers to design and manufacture miniaturized and low cost microwave components.

Branchline coupler is one of the most utilized microwave components in many radio frequency (RF) applications for convenience of design and system integration [3]. The branchline couplers are the key components for the RF microwave applications such as balanced amplifiers, mixers and phase shifters [4]. Branchline coupler (BLC) is a type of directional coupler which splits the incident power into two output power channels equally with 90˚ phase difference. In the branchline coupler, the phase difference between the coupled and through ports is odd multiplies of 90˚ [5]. Moreover, the conventional branchline coupler (BLC) is constructed with two through transmission lines (TLs) and two vertical branches which are quarter wavelength TLs. “Ever since the introduction of the branchline couplers, it has been a common practice to choose all the branches a quarter wavelength long at the center

of the frequency band of interest." [6]. However, at the frequencies below 10GHz, the quarter wavelength transmission lines (TLs) become physically too long; therefore the size of the branchline coupler consumes a large amount of chip area [5]. The usage of large sized microwave component becomes very difficult for designers to integrate the branchline coupler (BLC) into the microwave systems. In order to reduce the size of the branchline coupler, different kinds of techniques are presented in the literature.

In this thesis work, the purpose had been to design and fabricate a reduced size branchline coupler for X band monolithic microwave integrated circuits (MMICs) as to be explained step by step. Firstly, the theoretical analysis of the directional and branchline coupler (BLC) were performed. After that, miniaturization techniques were implemented to reduce the size of conventional branchline coupler. At the next stage, the miniaturized branchline coupler (mBLC) design was carried on utilizing the Agilent's Advanced Design System (ADS). Electromagnetic (EM) simulations were also performed by using the ADS Momentum 2.5D electromagnetic (EM) simulator. Then, to compare the accuracy of the simulators, the completed miniaturized branchline coupler designs were reconstructed and simulated by using the Sonnet Suites EM simulator. However, the EM simulation time period of Sonnet Suites turned out to be much longer than the EM simulation time period of ADS Momentum. During the design and simulation period, it was seen that there was a tradeoff between the EM simulation time period and accuracy of the design. Finally, the measured and simulated performances of the miniaturized branchline coupler (mBLC) were compared with each other.

In Chapter 2, an introduction to directional and hybrid couplers was given. The scattering parameters and ABCD parameter analysis of the directional and hybrid coupler were briefly described including the matrix representations, formulas of coupling and directivity of the couplers.

In Chapter 3, the branchline coupler (BLC) was discussed. In additional to this, the general properties of BLC will be described and formulas of BLC were derived from

the ABCD and scattering parameter matrices. Moreover, the miniaturization techniques were described and the theoretical analyses of the miniaturization techniques were performed.

In Chapter 4, the miniaturized branchline coupler designs were constructed in the Agilent's Advanced Design System (ADS) and their electromagnetic analysis were performed by using ADS Momentum 2.5D Method of Moment (MoM) based electromagnetic (EM) full wave solver. Then, the completed miniaturized branchline coupler designs were reconstructed in the Sonnet Suites, and their EM simulations performed in Sonnet EM Simulator which employs the rigorous Method of Moment analysis based on Maxwell's equations [8]. Moreover, the accuracy of EM simulations and the simulation time periods in both ADS Momentum EM simulator and Sonnet Suites EM simulator were compared.

In Chapter 5, S-parameter measurements of fabricated mBLC designs were performed and the measurement results of the mBLC design were presented. Then, EM simulation results of ADS Momentum and Sonnet Suites were compared with the S-parameter measurement results of the fabricated mBLCs.

Finally, the thesis was concluded in Chapter6 presenting the measurement results for the designed branchline couplers and making comments about the comparisons of the measurement results and the simulation results. In additional to conclusion, suggestions are also given for the further research directions.

CHAPTER 2

DIRECTIONAL COUPLER

2.1 Overview of Microwave Couplers

Couplers are passive devices that are widely utilized in microwave frequency applications, such as balanced amplifiers, antennas, mixers and phase shifters [4]. In additional to this, couplers are mostly used in the monolithic microwave integrated circuits (MMIC) to increase the gain flatness of the amplifier as well as dividing and combining the power. Moreover, general coupling mechanisms can be discussed into two main groups that are T-junctions and directional couplers [6]. T-junctions are three port networks that split the incident power into two output ports without having phase difference between the output ports. In contrast to this, the directional couplers are the four port networks that split the incident power into the output ports with arbitrary coupling ratio and phase difference between the output ports. Figure 2.1 illustrates the general power divider and power combiner block diagrams which can be either T-junctions or directional couplers with internally matched isolation port.

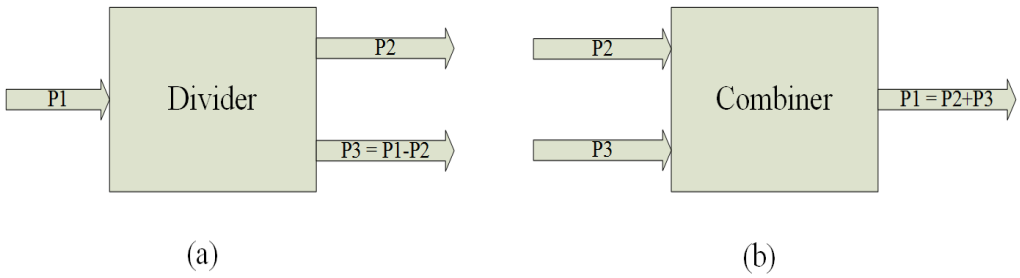

Figure 2.1 a) Power Divider b) Power Combiner

In the microwave frequency applications, couplers are preferred to use as a power divider and combiner as seen in the figure 2.1. In the divider mechanism, the coupler divides the incident power into the output ports with less power and phase difference between the output ports. In additional to this, couplers combines the incident powers from the two input ports into an output port. Furthermore, the remaining port of the coupler is used as an isolation port and isolation port is terminated with the characteristic impedance. When the output ports are terminated with the same characteristic impedance, for hybrid couplers, reflections from the output ports are summed up at the isolation port and cancelled at the input port.

There are different kinds of coupler design topologies which vary according to the design demands and application frequencies. Rat-race, coupled line and branchline coupler are special types of couplers which are constructed with the quarter wavelength TLs. In additional to this, one of the most used coupler type is branchline couplers (BLCs) which are designed with the two series and two shunt quarter wavelength transmission lines. BLC splits the incident power into the output ports with 90˚ phase difference between the output ports. Moreover, the phase difference and the operation frequency can be adjusted with the impedance and length of the both through TLs and branches. In the low frequencies, since the length of the quarter wavelength transmission lines are become quite long, the lumped elements are preferred to construct the coupling mechanism. So as to design the branchline coupler with lumped elements, TLs can be replaced with the inductors and capacitors. In contrast to this, in the higher frequencies the lumped element usage becomes a crucial problem. The resonance frequency of the lumped elements and having difficulties in the modeling the inductors accurately in the higher frequencies do not allow the designers to use lumped elements; because of this reason, in higher frequencies coplanar (CPW) and microstrip technologies are preferred to design the BLC. Furthermore, increasing the chip size leads to high costs in MMIC fabrication cost. Therefore, especially for BLCs utilized in MMICs, there are a variety of miniaturization techniques to reduce the sizes of the BLC such as π-shape, T-shape structures and meandering the transmission lines which were described in the following chapters.

2.2 Basics of Directional Coupler

Directional coupler is a four-port network that is widely utilized in the MMIC amplifier applications to split and combine the incident power. As the block diagram of the general directional coupler is given in the figure 2.2, it is mechanically and electrically symmetric.

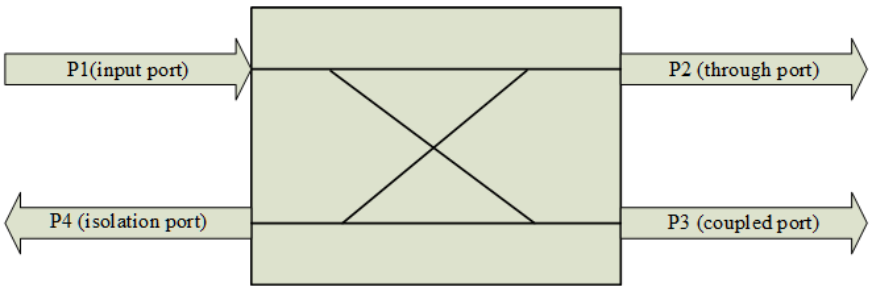

Figure 2.2: Block Diagram of Directional Coupler

Directional coupler splits the incident power into two output ports with arbitrary coupling ratio and the phase difference between the outputs can either 90˚ or 180˚. Moreover, the reflected power that is caused by mismatches is eliminated in the isolation port in order to prevent the reflections back to the input port.

As seen in the general block diagram of a directional coupler in the figure 2.2, the incident power is injected from the input port (Port 1), and then the incident power is splitted between the coupled and through ports. In the directional coupler, the input port and isolation port are uncoupled. Theoretically, directional couplers are four port networks, but in the commercial directional couplers, the isolation port is terminated with the load match internally. Therefore, there are three (3) ports in the commercial directional couplers.

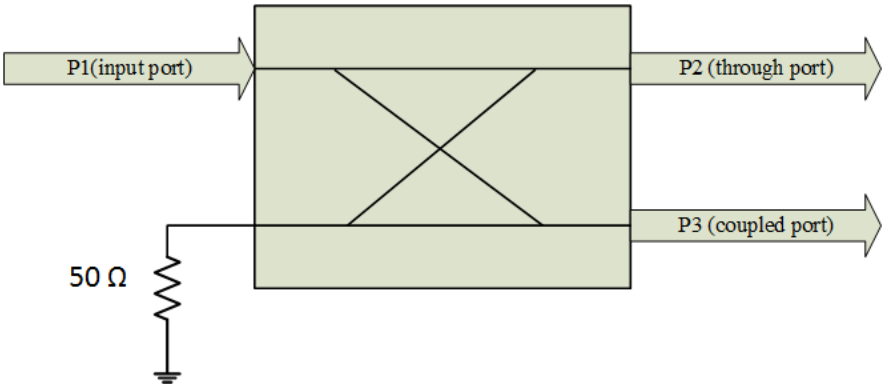

Figure 2.3: Block Diagram of Commercial Directional Coupler

Since directional coupler is a symmetrical network, the incident power can be excited from any port. For instance, if the incident power is excited to the port2; then the incident power will be splitted between the port1 and port4, and the port3 will be isolation port. A block diagram of this property is given in the figure 2.4.

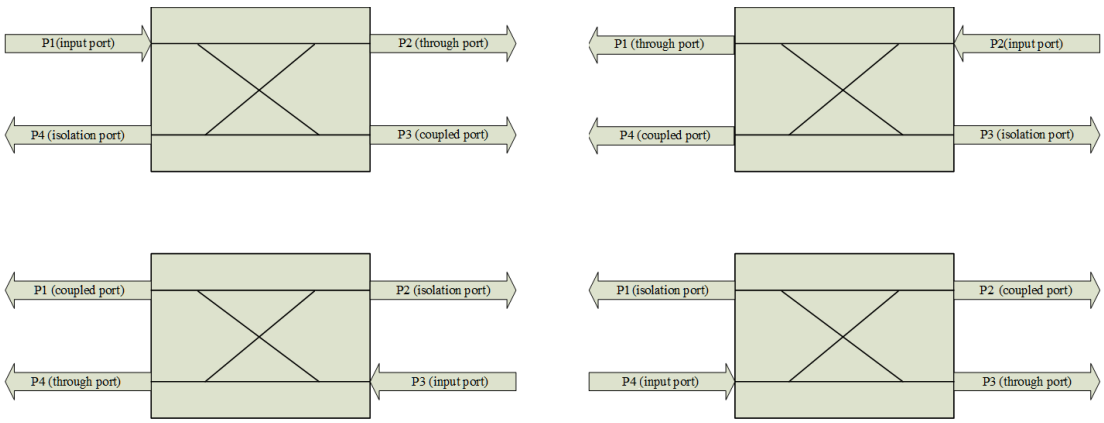

Figure 2.4: Directional Coupler Mechanisms

2.2.1 S-Parameters Analysis of Directional Couplers

In the microwave frequency applications, it can be easy to express the networks with the S-parameters. Since directional coupler is a four port network, [S] parameter matrix of the directional coupler can be defined with the sixteen independent elements. [S] matrix of directional coupler can be defined as:

$$[S] = \begin{bmatrix} S_{11} & S_{12} & S_{13} & S_{14} \\ S_{21} & S_{22} & S_{23} & S_{24} \\ S_{31} & S_{32} & S_{33} & S_{34} \\ S_{41} & S_{42} & S_{43} & S_{44} \end{bmatrix} \tag{2.1}$$

The ideal directional coupler is a lossless network and all the ports of the directional coupler are matched. In additional to this, a lossless scattering matrix becomes a unitary matrix. Therefore, all the diagonal elements ($S_{ii} = 0$) in the scattering matrix [S] become zero.

$$S_{11} = S_{22} = S_{33} = S_{44} = 0 \tag{2.2}$$

Thus, if we imply the unitary property into the [S]matrix that takes the following form:

$$[S] = \begin{bmatrix} 0 & S_{12} & S_{13} & S_{14} \\ S_{21} & 0 & S_{23} & S_{24} \\ S_{31} & S_{32} & 0 & S_{34} \\ S_{41} & S_{42} & S_{43} & 0 \end{bmatrix} \tag{2.3}$$

In ideal directional couplers, there is no coupling between the input (port 1) and isolation ports (port 4).

$$S_{14} = S_{41} = 0 \tag{2.4}$$

Also, there is no coupling between the through (port 2) and coupled (port 3) ports.

$$S_{23} = S_{32} = 0 \tag{2.5}$$

Then, if we apply the equations 2.4 and 2.5 into the [S] matrix, it takes the following form:

$$[S] = \begin{bmatrix} 0 & S_{12} & S_{13} & 0 \\ S_{21} & 0 & 0 & S_{24} \\ S_{31} & 0 & 0 & S_{34} \\ 0 & S_{42} & S_{43} & 0 \end{bmatrix} \tag{2.6}$$

[S] matrix of the lossless reciprocal directional coupler is symmetrical ($S_{ij} = S_{ji}$). If we imply the symmetric property into the [S] matrix and change the independent values with their equivalents, then the [S] matrix takes the following form:

$$[S] = \begin{bmatrix} 0 & S_{12} & S_{13} & 0 \\ S_{12} & 0 & 0 & S_{24} \\ S_{13} & 0 & 0 & S_{34} \\ 0 & S_{24} & S_{34} & 0 \end{bmatrix} \tag{2.7}$$

Unitary property implies that,

$$[S].[S]^* = [I] \tag{2.8}$$

Then, if we imply the unitary property into the [S] matrix, then we can obtain the following equation:

$$\begin{bmatrix} 0 & S_{12} & S_{13} & 0 \\ S_{12} & 0 & 0 & S_{24} \\ S_{13} & 0 & 0 & S_{34} \\ 0 & S_{24} & S_{34} & 0 \end{bmatrix} . \begin{bmatrix} 0 & S_{12}^* & S_{13}^* & 0 \\ S_{12}^* & 0 & 0 & S_{24}^* \\ S_{13}^* & 0 & 0 & S_{24}^* \\ 0 & S_{24}^* & S_{24}^* & 0 \end{bmatrix} = \begin{bmatrix} 1 & 0 & 0 & 0 \\ 0 & 1 & 0 & 0 \\ 0 & 0 & 1 & 0 \\ 0 & 0 & 0 & 1 \end{bmatrix} \tag{2.9}$$

After that, unitary scattering matrix satisfies the following equations 2.10-2.13.

$$|S_{12}|^2 + |S_{13}|^2 = 1 \tag{2.10}$$

$$|S_{12}|^2 + |S_{24}|^2 = 1 \tag{2.11}$$

$$|S_{13}|^2 + |S_{34}|^2 = 1 \tag{2.12}$$

$$|S_{24}|^2 + |S_{34}|^2 = 1 \tag{2.13}$$

With utilizing the equations 2.10 and 2.11, it can be derived that $|S_{13}|=|S_{24}|$. Similarly, with utilizing the equations 2.11 and 2.13, it can be derived that $|S_{12}|=|S_{34}|$. These equalities prove that the coupling between the port 1 and port 3 is equal to the coupling between the port 2 and port 4; as well as the coupling between the port 1 and port 2 is equal to coupling between port 3 and port 4.

$$|S_{13}| = |S_{24}| \tag{2.14}$$

$$|S_{12}| = |S_{34}| \tag{2.15}$$

So as to make the following analysis [7] simply, the phase differences can be choose as the following equations.

$$S_{12} = S_{34} = C_1 \tag{2.16}$$

$$S_{13} = C_2.\exp(j\theta) \tag{2.17}$$

$$S_{24} = C_2.\exp(j\varphi) \tag{2.18}$$

where C_1 and C_2 are real parameters and, φ and θ are phase constants.

The chosen simplifications for phase references can be implemented to the equations which are obtained by the unitary property.

$$|S_{12}|^2 + |S_{13}|^2 = 1 \;\rightarrow\; C_1^2 + C_2^2 = 1 \tag{2.19}$$

which results in [7]:

$$S_{12}^*.S_{13} + S_{24}^*.S_{34} = 0 \;\rightarrow\; \alpha\beta\exp(-j\theta) + \alpha\beta\exp(j\varphi) = 0$$

$$\rightarrow \alpha\beta\exp(-j\theta)[1 + \exp(j(\varphi + \theta)] = 0$$

$$\rightarrow \varphi + \theta = \pi \pm 2\pi n \tag{2.20}$$

After that the directional coupler can be grouped into two main groups according to the phase difference between the output ports. In order to divide the incident power into the outputs with equally, the phase differences can be chosen equal or unequal to each other. If the phase differences are equal to each other, the phase difference between the output ports can be determined as 90 ˚, otherwise the phase difference can be determined as 180 ˚ with using the equation 2.20.

1. 90˚ Hybrid Coupler: In this type of the coupler, the amplitude of the phase differences are equal, and $\varphi = \theta = \pi/2$. Then the [S] matrix becomes:

$$[S] = \begin{bmatrix} 0 & C_1 & jC_2 & 0 \\ C_1 & 0 & 0 & jC_2 \\ jC_2 & 0 & 0 & C_1 \\ 0 & jC_2 & C_1 & 0 \end{bmatrix} \tag{2.21}$$

2. 180˚ Hybrid Coupler: In this type of the coupler, the amplitude of the phase differences are chosen with π apart from each other, $\varphi = 0, \quad \theta = \pi$. Then the [S] matrix of 180 ˚ hybrid coupler becomes:

$$[S] = \begin{bmatrix} 0 & C_1 & C_2 & 0 \\ C_1 & 0 & 0 & -C_2 \\ C_2 & 0 & 0 & C_1 \\ 0 & -C_2 & C_1 & 0 \end{bmatrix} \tag{2.22}$$

2.3 Hybrid Couplers

Hybrid couplers are a special type of a directional coupler. In the directional couplers, the power division between the output ports can be arbitrarily designed according to the design requirements; yet in the hybrid couplers the power divisions between the output ports are equal. In other words, the hybrid couplers split the incident power equally to the output ports. Because of this reason, hybrid couplers

are also known as 3dB hybrid couplers. The equal power division is satisfied with taking

$$C_1 = C_2 = \frac{1}{\sqrt{2}} \tag{2.23}$$

Hybrid couplers are grouped into the two main subgroups according to the phase differences between the output ports as 90˚ and 180˚ hybrid couplers.

2.3.1 90˚ Hybrid Couplers (3dB)

90˚ hybrid coupler is a 3dB directional coupler with the 90˚ phase difference at the output ports. This type of coupler is generally known as quadrature coupler. The quadrature couplers equally split the incident power between the output ports with 90˚ phase difference.

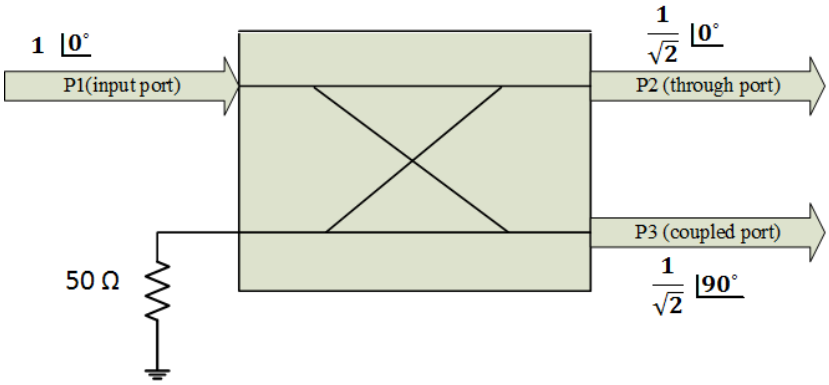

Figure 2.5: 90˚ Hybrid Coupler (3dB)

In the figure 2.5, the general block diagram of the 90˚ hybrid coupler (3dB) is given. As seen in the figure 2.5, the power is injected at the input port (P1) and then coupler equally splits the incident power to the through (P2) and coupled (P3) ports with the 90˚ phase difference, and the isolation port (P4) is internally terminated with the match load so as to eliminate the reflected power because of mismatches. The scattering matrix [S] of the 90˚ hybrid coupler has the form

$$[S] = \frac{1}{\sqrt{2}}\begin{bmatrix} 0 & 1 & j & 0 \\ 1 & 0 & 0 & j \\ j & 0 & 0 & 1 \\ 0 & j & 1 & 0 \end{bmatrix} \quad (2.24)$$

90˚ Hybrid couplers are used in many applications in microwave applications such as RF amplifiers, test and measurement, transmitters and receivers. According to attributes of the different application fields, there are different types of quadrature couplers such as the branchline coupler, Lange coupler, overlay coupler and edge coupler.

2.3.2 180˚ Hybrid Couplers (3dB)

180˚ hybrid coupler is a 3dB directional coupler with the 180˚ phase difference at the output ports. This type of hybrid couplers equally split the incident power between the output ports with 180˚ phase difference.

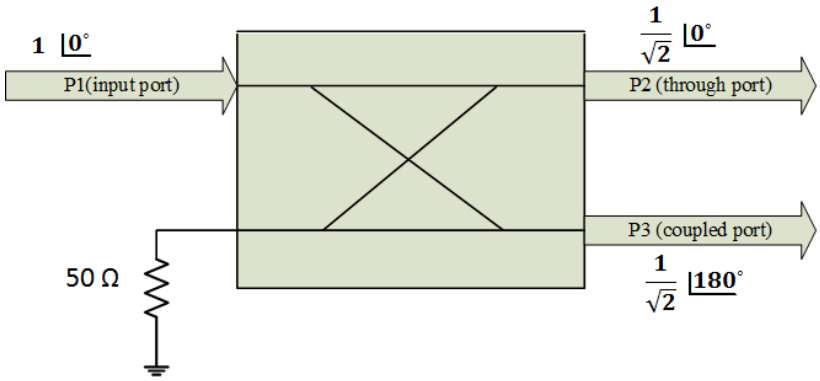

Figure 2.6: 180˚ Hybrid Coupler (3dB)

In the figure 2.6, the general diagram of the 180˚ hybrid coupler (3dB) is given. According to the figure 2.6, the power is injected at the input port (P1) and then coupler equally splits the incident power to the through (P2) and coupled (P3) ports with the 180˚ phase difference, and the isolation port (P4) is internally terminated with the match load so as to eliminate the reflected power because of mismatches. The scattering matrix [S] of the 180˚ hybrid coupler has the form

$$[S] = \frac{1}{\sqrt{2}} \begin{bmatrix} 0 & 1 & 1 & 0 \\ 1 & 0 & 0 & -1 \\ 1 & 0 & 0 & 1 \\ 0 & -1 & 1 & 0 \end{bmatrix} \tag{2.25}$$

As the 90 hybrid coupler, 180˚ hybrid couplers are used in many applications in microwave applications such as RF amplifiers, test and measurement, transmitters and receivers. According to attributes of the different application fields, there are different types of 180˚ hybrid couplers such as rate-race coupler and magic tee coupler.

CHAPTER 3

SYNTHESIS OF MINIATURIZED BRANCHLINE COUPLERS

Hybrid couplers are passive microwave devices that are widely utilized for power division and power combination in many RF microwave circuit applications such as balanced amplifiers, balanced mixers [13] and so forth. There are different types of hybrid coupler design topologies [14] with coplanar waveguide, microstrip or strip transmission line technologies such as branchline couplers, Lange couplers, rate-race couplers and coupled line couplers. Each type of the hybrid couplers has different advantages and disadvantages in comparison with each other. In order to choose the appropriate type of coupler, the design parameters such as coupling ratio, directivity, isolation, phase difference, bandwidth and the size of the coupler have important role on designer's choice. In the RF microwave circuit design, the branchline coupler (BLC) is mostly preferred devices by the designers because of being easy to design and cost effective. However, the hybrid coupler topologies utilize quarter wavelength TLs and the size of the hybrid couplers become a crucial problem for the designers. Thus, the size of the hybrid couplers need to be reduced for designs to satisfy the application requirements.

In this chapter, the general properties of the conventional branchline hybrid couplers and miniaturization techniques will be discussed. The idea of the miniaturization techniques depends on the replacing the quarter wavelength transmission lines with using equivalent circuits in T-shape and π-shape structures so as to obtain significant size reduction [12]. Finally, the mostly used method of meandering the transmission line will be discussed.

3.1 The Conventional Branchline Hybrid Coupler

The conventional branchline coupler is the fundamental components of the microwave circuits. The branchline coupler is a 3dB directional coupler with 90˚ phase difference between the two output ports and it can be designed with using the coplanar waveguide (CPW) and microstrip technologies. The scattering [S] matrix of the conventional branchline coupler is given in the equation (3.1).

$$[S] = \frac{1}{\sqrt{2}} \begin{bmatrix} 0 & 1 & j & 0 \\ 1 & 0 & 0 & j \\ j & 0 & 0 & 1 \\ 0 & j & 1 & 0 \end{bmatrix} \tag{3.1}$$

The conventional branchline coupler is constructed with four quarter wavelength TLs in square shape. As seen in the figure 3.1, for the conventional branchline hybrid coupler, horizontal quarter wavelength impedance transformers have the characteristic impedance of Z_{01} and the vertical quarter wavelength impedance transformers have the characteristic impedance of Z_{02}. In additional to this, all the ports are designed to be matched to load impedance with the characteristic impedance of Z_0.

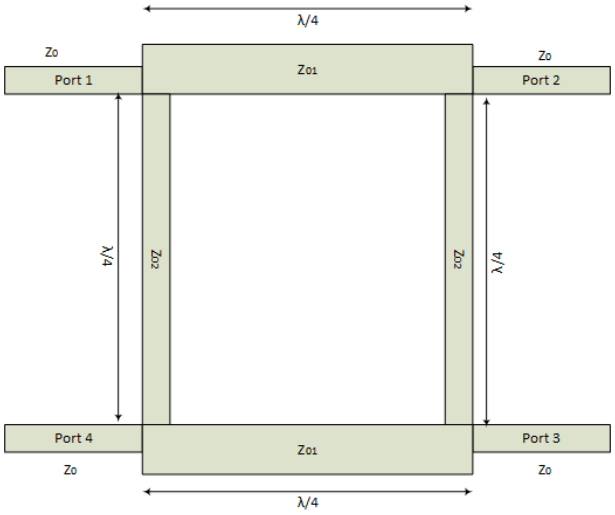

Figure 3.1: The Conventional Branchline Coupler

According to the general geometry of the conventional branchline coupler as seen in the figure 3.1, the incident power is applied to the input port (P1) and the incident power is splitted equally between the through (P2) and coupled (P3) ports with the 90˚ phase difference. The isolation port (P4) is terminated with the load impedance Z_0.

3.2 Theoretical Analysis of the Branchline Coupler

In RF microwave circuit design, it is the easy way to define the microwave network with using S-parameters. In order to derive the S-parameter matrix, even-odd mode approach is used [15]. As seen in the schematic of the branchline coupler in the figure 3.2, all ports are matched to the characteristic impedances of Z_0.

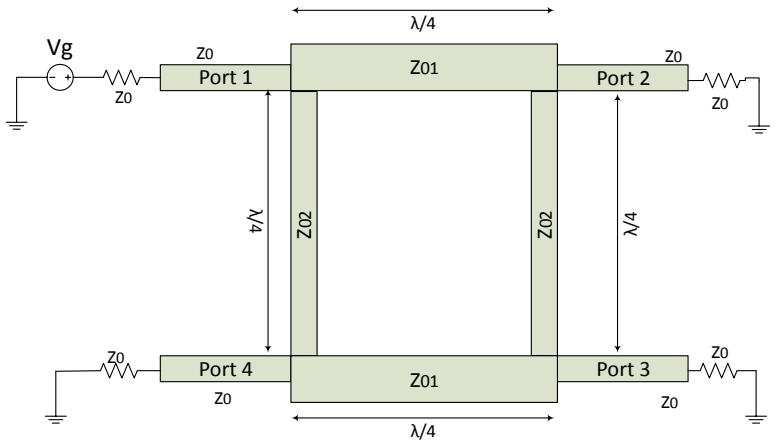

Figure 3.2: The schematic of the branchline coupler

In order to determine the characteristic impedances of the transmission lines, firstly the conventional branchline coupler was cut into the two pieces symmetrically. As seen in the figure 3.3, there is a horizontal line that splits the branchline coupler symmetrically. The polarizations of the applied voltage supplies are defined so as to

make sure that there is zero voltage at the isolation port and there is Vg voltage at the input port.

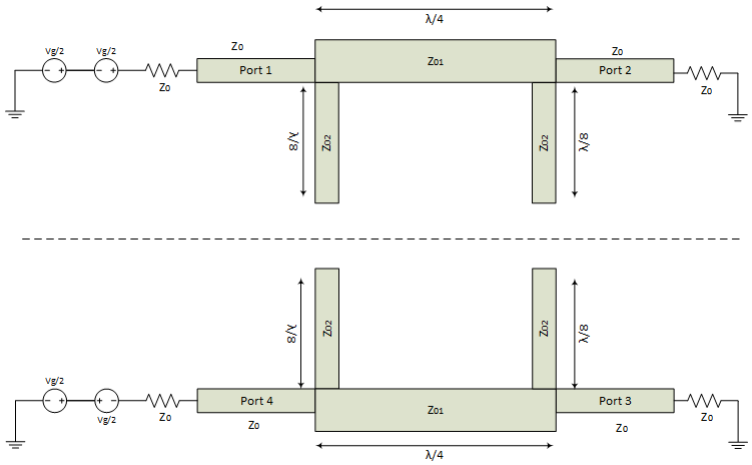

Figure 3.3: Even /Odd Mode Analysis of BLC

In the even mode analysis, there is a magnetic wall between the splitted parts of the branchline coupler. The magnetic wall behaves as the open circuit and the splitted transmission lines work as an open stub. In additional to this, the voltage polarity of each part is same to each other. The schematic of the even mode analysis of the branchline coupler is given in the figure 3.4.

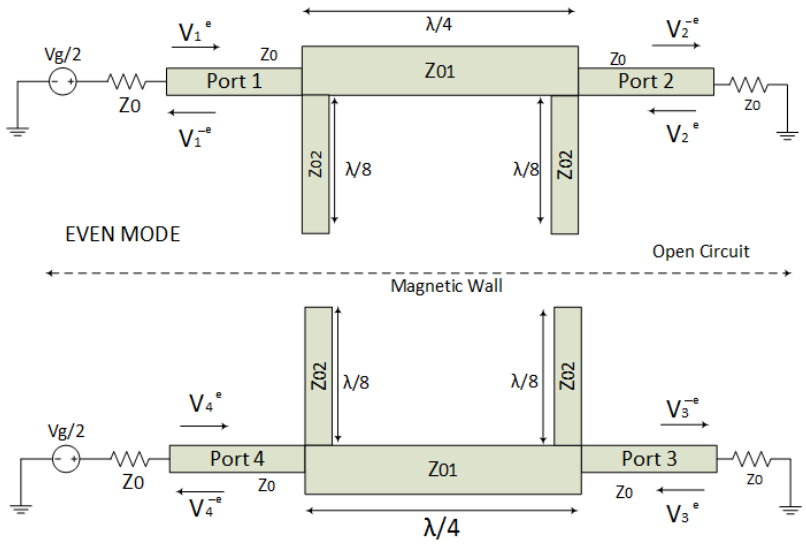

Figure 3.4: Even Mode Analysis of BLC

In odd mode analysis, there is an electrical wall between the splitted parts of the branchline coupler. Since the electrical wall is behaving as a short circuit, splitted transmission lines work as a short stub. In additional to this, the magnitude of the voltage is equal; but in the opposite polarity to each other. The schematic of the odd mode analysis of the branchline coupler is given in the figure 3.5.

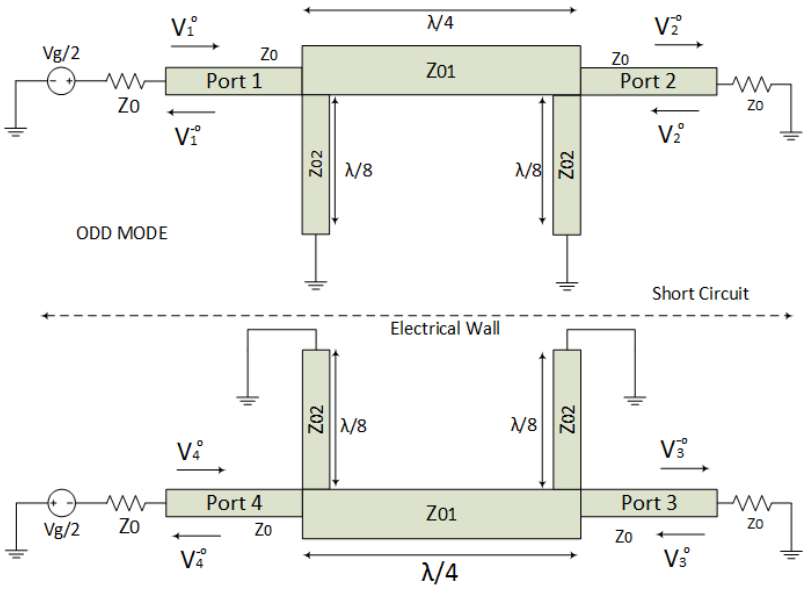

Figure 3.5: Odd Mode Analysis of BLC

In even mode analysis, BLC is divided into two pieces symmetrically and it behaves as there is a magnetic wall between the pieces. Moreover, as seen in the figure 3.6, each piece has the equal characteristic impedance as well as the equal voltage values with same polarity.

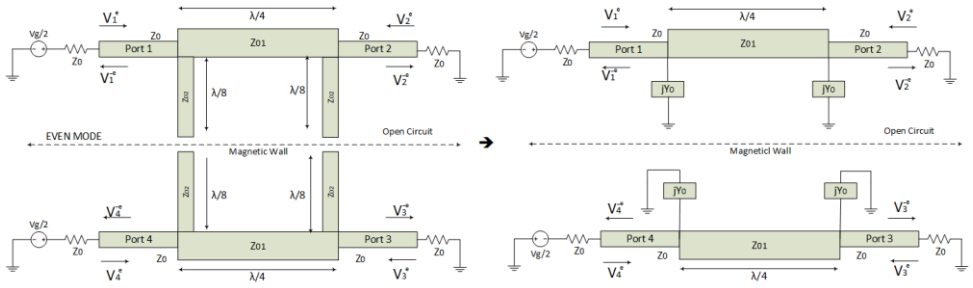

Figure 3.6: Even Mode Analysis of BLC and Equivalent Circuit

Therefore, the voltage values of the each port can be expressed for the even mode as followings:

$$V_1^e = V_4^e \tag{3.1}$$

$$V_2^e = V_3^e \tag{3.2}$$

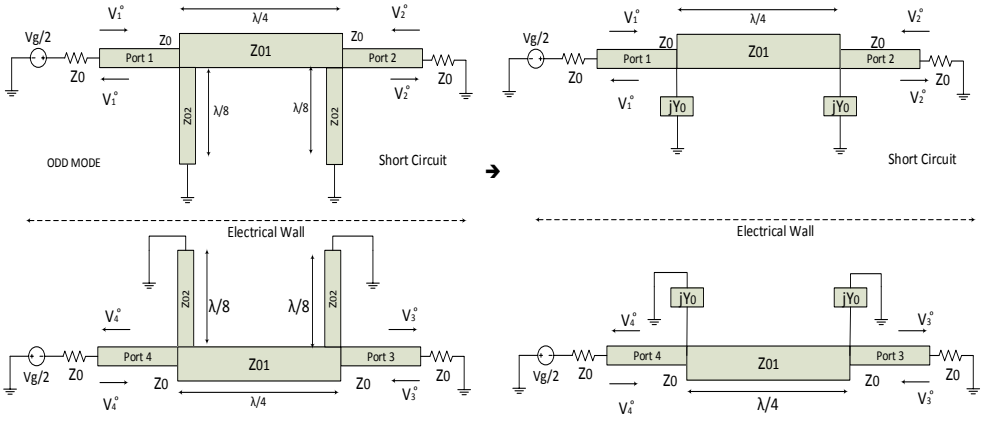

Figure 3.7: Odd Mode Analysis of BLC and Equivalent Circuit

In odd mode analysis, the BLC is divided symmetrically into two pieces. In additional to this, each piece has the equal characteristic impedance as well as the equal voltage value; but in the opposite polarities. Therefore, the voltage values of the each port can be expressed for the odd mode as followings:

$$V_1^o = -V_4^o \tag{3.3}$$

$$V_2^o = -V_3^o \tag{3.4}$$

With using the even-odd mode analysis approach, incident and reflected voltage values of each port can be determined as seen in the Table 3.1. Γ is the reflection coefficient and T is the transmission coefficients. In additional to this, "e" and "o" letters denotes even and odd mode respectively.

Table 3.1: The incident and reflected voltage values of each port in branchline coupler [16]

	EVEN MODE		ODD MODE	
	Incident	Reflected	Incident	Reflected
1st Port	V_1^{+e}	$V_1^{-e} = \Gamma_{1.}^e V_1^{+e}$	$V_1^{+o} = V_1^{+e}$	$V_1^{-o} = \Gamma_1^o V_1^{+o}$
2nd Port	$V_2^{+e} = 0$	$V_2^{-e} = T_{34}^e V_1^{+e}$	$V_2^{+o} = 0$	$V_2^{-o} = T_{34}^o V_1^{+o}$
3rd Port	$V_3^{+e} = V_1^{+e}$	$V_3^{-e} = \Gamma_3^e V_3^{+e}$	$V_3^{+o} = -V_1^{+e}$	$V_3^{-o} = \Gamma_3^o V_3^{+o}$
4th Port	$V_4^{+e} = 0$	$V_4^{-e} = T_{21}^e V_1^{+e}$	$V_4^{+o} = 0$	$V_4^{-o} = T_{21}^o V_1^{+o}$

If we apply superposition, the incident and reflected voltage values of the input port is given in equations 3.5 and 3.6 respectively.

$$V_i^- = V_i^{-e} + V_i^{-o} \text{ where } i = 1, 2, 3, 4 \tag{3.5}$$

$$V_i^+ = V_i^{+e} + V_i^{+o} \text{ where } i = 1, 2, 3, 4 \tag{3.6}$$

The reflection coefficients and transmission coefficient of the each port for even and odd mode can be expressed as following equations.

$$\Gamma_1^e = \Gamma_3^e \tag{3.7}$$

$$\Gamma_1^o = \Gamma_3^o \tag{3.8}$$

$$T_{21}^e = T_{34}^e \tag{3.9}$$

$$T_{21}^o = T_{34}^o \tag{3.10}$$

Then, in order to calculate the incident and reflected voltage values of the each port, equations 3.5 and 3.6 are applied. The incident and reflected voltage values of the each port can be derived as following:

$$V_1^+ = V_1^{+e} + V_1^{+o} = V_1^{+e} + V_1^{+e} = 2V_1^{+e} \tag{3.11}$$

$$V_1^- = \Gamma_1^e V_1^{+e} + \Gamma_1^o V_1^{+o} = V_1^{+e}(\Gamma_1^e + \Gamma_1^o) \tag{3.12}$$

$$V_2^+ = 0 \tag{3.13}$$

$$V_2^- = T_{21}^e V_1^{+e} + T_{21}^o V_1^{+o} = V_1^{+e}(T_{21}^e + T_{21}^o) \tag{3.14}$$

$$V_3^+ = V_1^{+e} - V_1^{+e} = 0 \tag{3.15}$$

$$V_3^- = \Gamma_1^e V_1^{+e} - \Gamma_1^o V_1^{+e} = V_1^{+e}(\Gamma_1^e - \Gamma_1^o) \tag{3.16}$$

$$V_4^+ = 0 \tag{3.17}$$

$$V_4^- = V_1^{+e}(T_{41}^e - T_{41}^o) = V_1^{+e}(T_{41}^e - T_{41}^o) \tag{3.18}$$

Then the [ABCD] matrix of the even and odd mode transmission lines with characteristic impedance of Z_0^e and Z_0^o and lenght l, can be expressed as [7] in the equations (3.19) and (3.20).

For even mode:

$$\begin{bmatrix} A_e & B_e \\ C_e & D_e \end{bmatrix} = \begin{bmatrix} \cos(\beta l) & jZ_0^e \sin(\beta l) \\ \frac{j\sin(\beta l)}{Z_0^e} & \cos(\beta l) \end{bmatrix} \tag{3.19}$$

For odd mode:

$$\begin{bmatrix} A_o & B_o \\ C_o & D_o \end{bmatrix} = \begin{bmatrix} \cos(\beta l) & jZ_0^o \sin(\beta l) \\ \frac{j\sin(\beta l)}{Z_0^o} & \cos(\beta l) \end{bmatrix} \tag{3.20}$$

where $\beta = \omega/c$ is the phase constant.

In the even and odd mode analysis, the divided parts of the branchline coupler can be defined with the parallel open and short stubs. In additional to this, in the even odd mode approach, the open and short stubs are λ/8 wavelength transmission lines. In the even odd mode analysis of BLC, the characteristic impedance of the serial quarter wavelength Z_{01} is equal to $Z_0/\sqrt{2}$ and the characteristic impedance of the shunt quarter wavelength Z_{02} is equal to Z_0. Figure 3.8 shows the general equivalent circuit of splitted BLC.

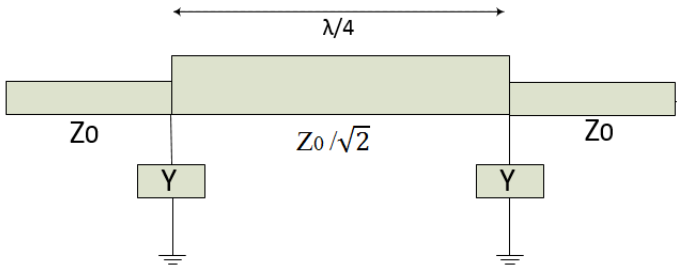

Figure 3.8: The General Equivalent Circuit of the Splitted BLC

If we consider the equivalent circuits for the even and odd mode configuration when $Z_{01} = Z_0/\sqrt{2}$ and $Z_{02} = Z_0$, the general equivalent circuit of splitted BLC can be seen in the figure 3.8.

$$Y = \begin{cases} -jY_0, & \text{for odd mode} \\ jY_0, & \text{for even mode} \end{cases} \tag{3.21}$$

In the even-odd mode analysis, the two port [ABCD] matrix excitations can be done with the multiplications of three elements as seen in the figure 3.8.

$$\begin{bmatrix} A & B \\ C & D \end{bmatrix} = \begin{bmatrix} A & B \\ C & D \end{bmatrix}_Y \begin{bmatrix} A & B \\ C & D \end{bmatrix}_{\frac{\lambda}{4}\, line} \begin{bmatrix} A & B \\ C & D \end{bmatrix}_Y \tag{3.22}$$

Then the [ABCD] matrix for the even mode excitation can be derived as

$$\begin{bmatrix} A & B \\ C & D \end{bmatrix} = \begin{bmatrix} 1 & 0 \\ Y & 1 \end{bmatrix}_Y \begin{bmatrix} 0 & \frac{jZ_o}{\sqrt{2}} \\ \frac{j\sqrt{2}}{Z_o} & 0 \end{bmatrix}_{\frac{\lambda}{4}\, line} \begin{bmatrix} 1 & 0 \\ Y & 1 \end{bmatrix}_Y$$

$$= \begin{bmatrix} 1 & 0 \\ Y & 1 \end{bmatrix}_Y \begin{bmatrix} \frac{jZ_oY}{\sqrt{2}} & \frac{jZ_0}{\sqrt{2}} \\ \frac{j\sqrt{2}}{Z_0} & 0 \end{bmatrix}$$

$$= \begin{bmatrix} \frac{jZ_0Y}{\sqrt{2}} & \frac{jZ_0}{\sqrt{2}} \\ \frac{j\sqrt{2}}{Z_0} + \frac{jZ_0Y^2}{\sqrt{2}} & \frac{jZ_0Y}{\sqrt{2}} \end{bmatrix} \tag{3.23}$$

Substitute the equation 3.21 into the equation 3.23.

For even mode:

$$\begin{bmatrix} A & B \\ C & D \end{bmatrix}_e = \frac{1}{\sqrt{2}} \begin{bmatrix} 1 & jZ_0 \\ j\left(\frac{1}{Z_0}\right) & 1 \end{bmatrix} \tag{3.24}$$

For odd mode:

$$\begin{bmatrix} A & B \\ C & D \end{bmatrix}_o = \frac{1}{\sqrt{2}} \begin{bmatrix} 1 & -jZ_0 \\ -j\left(\frac{1}{Z_0}\right) & 1 \end{bmatrix} \tag{3.25}$$

After the [ABCD] matrices had been obtained for even and mode excitation, the [ABCD] parameters were converted into the [S] parameters with using the conversion of [ABCD] parameters to [S] parameters. The [S] parameter matrix for the even and odd mode excitations is given as:

For even mode:

$$[S]_e = \begin{bmatrix} 0 & \frac{1-j}{\sqrt{2}} \\ \frac{1-j}{\sqrt{2}} & 0 \end{bmatrix} \tag{3.26}$$

For odd mode:

$$[S]_o = \begin{bmatrix} 0 & \frac{-1-j}{\sqrt{2}} \\ \frac{-1-j}{\sqrt{2}} & 0 \end{bmatrix} \tag{3.27}$$

With using the [S] parameters matrices that are obtained from even odd mode analysis, the s-parameters of the branchline coupler can be derived.

$$S_{11} = \left.\frac{V_1^-}{V_1^+}\right|_{a_2=a_3=a_4=0} \rightarrow S_{11} = \frac{V_1^{-e} + V_1^{-o}}{V^+ + V^+} = \frac{1}{2}\left(\frac{V_1^{-e}}{V^+} + \frac{V_1^{-o}}{V^+}\right) = \frac{1}{2}\left(S_{11}^e + S_{11}^o\right)$$
$$= 0$$

Hence $S_{11} = 0$ by symmetry: $S_{11} = S_{22} = S_{33} = S_{44} = 0$

$$S_{21} = \left.\frac{V_2^-}{V_1^+}\right|_{a_2=a_3=a_4=0} \rightarrow S_{21} = \frac{V_2^{-e} + V_2^{-o}}{V^+ + V^+} = \frac{1}{2}\left(\frac{V_2^{-e}}{V^+} + \frac{V_2^{-o}}{V^+}\right)$$
$$= \frac{1}{2}\left(S_{21}^e + S_{21}^o\right)$$
$$= \frac{1}{2}\left[\left(\frac{-1-j}{\sqrt{2}}\right) + \left(\frac{-1-j}{\sqrt{2}}\right)\right] = \frac{-j}{\sqrt{2}}$$

Hence $S_{21} = \frac{-j}{\sqrt{2}}$ by symmetry and reciprocity: $S_{21} = S_{12} = S_{43} = S_{34} = \frac{-j}{\sqrt{2}}$

$$S_{31} = \left.\frac{V_3^-}{V_1^+}\right|_{a_2=a_3=a_4=0} \rightarrow S_{31} = \frac{V_3^{-e} + V_3^{-o}}{V^+ + V^+} = \frac{1}{2}\left(\frac{V_3^{-e}}{V^+} + \frac{V_3^{-o}}{V^+}\right)$$

$$= \frac{1}{2}\left(S_{21}^e - S_{21}^o\right)$$

$$= \frac{1}{2}\left[\left(\frac{-1-j}{\sqrt{2}}\right) - \left(\frac{-1-j}{\sqrt{2}}\right)\right] = \frac{-1}{\sqrt{2}}$$

Hence $S_{31} = \frac{-1}{\sqrt{2}}$ by symmetry and reciprocity: $S_{31} = S_{13} = S_{24} = S_{42} = \frac{-1}{\sqrt{2}}$

$$S_{41} = \left.\frac{V_4^-}{V_1^+}\right|_{a_2=a_3=a_4=0} \rightarrow S_{41} = \frac{V_4^{-e} + V_4^{-o}}{V^+ + V^+} = \frac{1}{2}\left(\frac{V_1^{-e}}{V^+} - \frac{V_1^{-o}}{V^+}\right) = \frac{1}{2}\left(S_{11}^e - S_{11}^o\right)$$

$$= 0$$

Hence $S_{41} = 0$ by symmetry and reciprocity: $S_{41} = S_{14} = S_{23} = S_{32} = 0$

After the each S-parameter values had calculated, [S] matrix of the branchline coupler is shaped as:

$$[S] = \frac{-1}{\sqrt{2}}\begin{bmatrix} 0 & j & 1 & 0 \\ j & 0 & 0 & 1 \\ 1 & 0 & 0 & j \\ 0 & 1 & j & 0 \end{bmatrix} \tag{3.28}$$

As a result of even odd mode analysis, BLC divides the incident power into the output ports with 90 phase difference between the output ports. In additional to this, the port1 and port4 are uncoupled ports, as well as the port2 and port3 are uncoupled.

3.2.1 Properties of BLC

The performance of the BLC can be stated with the coupling, isolation and directivity. The coupling ratio is one of the most important parameter of BLC. In additional to this, the coupling ratio represents the fraction between the input power and output power. Moreover, BLC can be called according to their maximum coupling ratio. The coupling in decibel (dB) can be defined as in the equation 3.29.

$$C = 10 \log \frac{P1}{P3} \tag{3.29}$$

The directivity is an important parameter that shows how well the BLC isolates the travelling power between the output ports. The directivity in decibel (dB) can be defined as in the equation 3.30.

$$D = 10 \log \frac{P3}{P4} \tag{3.30}$$

Isolation represents the fraction between the input power and power out at the isolation port. Isolation in decibel (dB) can be defined as in the equation 3.31.

$$I = 10 \log \frac{P1}{P4} \tag{3.31}$$

3.3 New Design Approach

The conventional branchline coupler are key subsystems in the RF microwave circuits because of having a various application fields such as balanced amplifiers, mixers, wireless systems array antennas etc. The conventional branchline couplers are composed of four quarter wavelength transmission line that covers a large amount of area and the operation frequency bandwidth limited by the quarter wavelength TLs. At the low frequencies in the microwave frequencies, the size of the branchline coupler becomes larger; because the length of the quarter wavelength transmission line is inversely proportional to the frequency. Therefore, in the microwave circuit design the large sized branchline coupler increases the cost of the

circuit and also it will be difficult for designer to integrate the branchline coupler into the microwave systems. In order to reduce the size of the branchline coupler, quarter wavelength TLs are replaced with equivalent circuits and it is called as miniaturization. There are different kinds of miniaturization techniques which can be listed as lumped element technique, T-shape structures, π-shape structures and meander section. In the following subsection the different type of miniaturization techniques will be discussed.

3.3.1 Lumped Element Technique

Lumped element technique is one of the most used techniques to reduce the size of the branchline coupler. In the lumped element technique, the quarter wavelength transmission lines are replaced with the spiral inductor and lumped capacitors. This technique is mostly used in the low frequencies; because in the high frequency applications it is very difficult to have a precious spiral inductor models and the resonance frequency of the lumped elements restrict the high frequency applications. Moreover, the sensitivity and losses of the lumped elements limits the high frequency applications [9]. Therefore, the lumped element technique generally preferred in low frequency applications.

3.3.2 T-shape Structures

In T-shape structures methodology, we aim to miniaturize the quarter wavelength transmission lines and widen the operation frequency bandwidth. In order to achieve this purposes, the horizontal and vertical quarter wavelength transmission line are replaced with the T-shape structures. In this technique, T-shaped structure is implemented in to the branchline coupler design as shown in the figure 3.9.

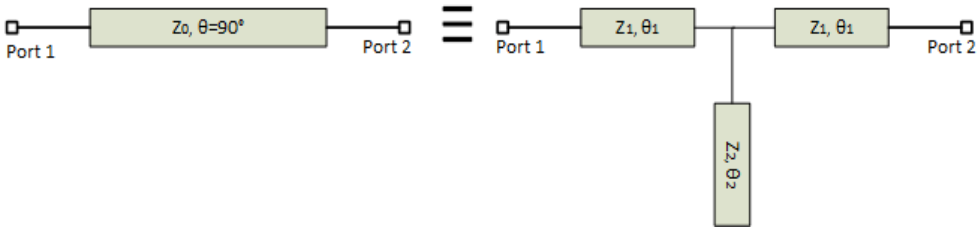

Figure 3.9: a) λ/4 Transmission Line b) T-shaped Structure Equivalent to (a)

In the T-shaped equivalent circuit, (Z_2, θ_2) is an open circuited stub and in order to find the [ABCD] matrix of the open circuited stub is replaced with the shunt stop. The circuit representation of the shunt open stub is given in the figure 3.10.

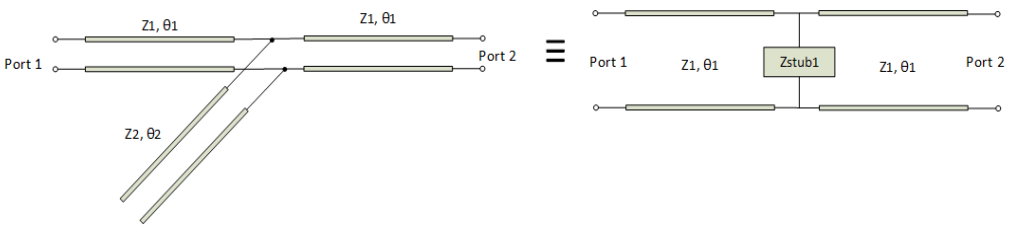

Figure 3.10: T-shaped Structure Circuit Representations

In the circuit representation of the T-shaped structure, the characteristic impedance of the open stub is given as:

$$Z_{stub1} = -j\frac{Z_2}{\tan(\theta_2)} \tag{3.32}$$

The [ABCD] matrix of the quarter wavelength transmission line as seen in the figure2.8 (a) can be written as:

$$\begin{bmatrix} A & B \\ C & D \end{bmatrix}_{\lambda/4} = \begin{bmatrix} 0 & jZ_0 \\ jY_0 & 0 \end{bmatrix} \tag{3.33}$$

The [ABCD] matrix of the T-shaped equivalent circuit is described as follow:

$$M_T = M_1 . M_2 . M_1 \tag{3.34}$$

where M_1 is the series components and M_2 is the shunt components of the T-shaped structure that is seen in the figure 3.10 (b).

$$M_1 = \begin{bmatrix} \cos(\theta_1) & jZ_1 \sin(\theta_1) \\ jY_1 \sin(\theta_1) & \cos(\theta_1) \end{bmatrix} \tag{3.35}$$

$$M_2 = \begin{bmatrix} 1 & 0 \\ jY_2 \tan(\theta_2) & 1 \end{bmatrix} \tag{3.36}$$

Substituting the (3.33), (3.35) and (3.36) in to the (3.34)

$$\begin{bmatrix} 0 & jZ_0 \\ jY_0 & 0 \end{bmatrix} = \begin{bmatrix} \cos(\theta_1) & jZ_1 \sin(\theta_1) \\ jY_1 \sin(\theta_1) & \cos(\theta_1) \end{bmatrix} \begin{bmatrix} 1 & 0 \\ jY_2 \tan(\theta_2) & 1 \end{bmatrix} \begin{bmatrix} \cos(\theta_1) & jZ_1 \sin(\theta_1) \\ jY_1 \sin(\theta_1) & \cos(\theta_1) \end{bmatrix} \tag{3.37}$$

After expanding the above expression, the term in the [ABCD] matrix can be written as

$$A = \cos^2\theta_1 - \sin^2\theta_1 - \frac{Z_1}{Z_2} \sin\theta_1 \cos\theta_1 \tan\theta_2 \tag{3.38}$$

$$B = j2Z_1 \sin\theta_1 \cos\theta_1 - j \frac{Z_1^2}{Z_2} \sin^2\theta_1 \tan\theta_2 \tag{3.39}$$

$$C = j\frac{2}{Z_1} \sin\theta_1 \cos\theta_1 + j \frac{1}{Z_2} \cos^2\theta_1 \tan\theta_2 \tag{3.40}$$

$$D = \cos^2\theta_1 - \sin^2\theta_1 - \frac{Z_1}{Z_2} \sin\theta_1 \cos\theta_1 \tan\theta_2 \tag{3.41}$$

By evaluating the [ABCD] matrix, the following equations are obtained:

$$Z_1 = \cot\theta_1 . \frac{1-\cos\theta_0}{\sin\theta_0} . Z_0 \tag{3.42}$$

$$Z_2 = \tan\theta_2 . \frac{\cos^2\theta_1}{\cos 2\theta_1 - \cos\theta_0} . \frac{1-\cos\theta_0}{\sin\theta_0} . Z_0 \tag{3.43}$$

3.3.3 π-shape Structures

In the π-shaped structure methodology, it is aimed to miniaturize the quarter wavelength transmission lines and widen the operation bandwidth as similar as in the T-shaped structure methodology. In this technique, the horizontal and vertical quarter wavelength transmission lines are replaced with the π-shaped structures. The implementation of the π-shaped structures into the branchline coupler design is given in the figure 3.11.

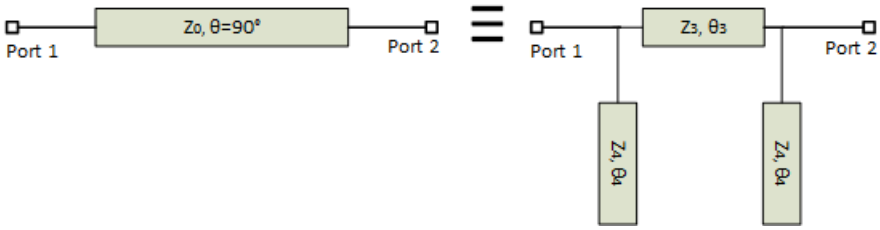

Figure 3.11: a) λ/4 Transmission Line b) π-shaped Structure Equivalent to (a)

In the π-shaped equivalent circuit, (Z_3, θ_3) is the series transmission line and (Z_4, θ_4) are the open circuited stubs and in order to find the [ABCD] matrix of the open circuited stubs are replaced with the shunt stops. The circuit representation of the shunt open stub is given in the figure 3.12.

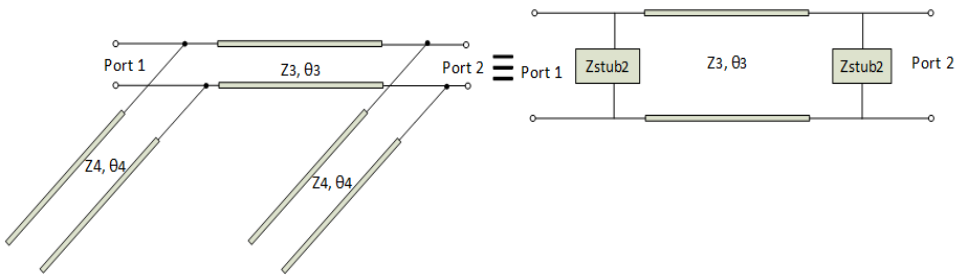

Figure 3.12: π-shaped Structure Circuit Representations

In the circuit representation of the T-shaped structure, the characteristic impedance of the open stub is given as:

$$Z_{stub2} = -j\frac{Z_4}{\tan(\theta_4)} \tag{3.44}$$

The [ABCD] matrix of the quarter wavelength transmission line as seen in the figure2.10 (a) can be written as:

$$\begin{bmatrix} A & B \\ C & D \end{bmatrix}_{\lambda/4} = \begin{bmatrix} 0 & jZ_0 \\ jY_0 & 0 \end{bmatrix} \tag{3.45}$$

The [ABCD] matrix of the π-shaped equivalent circuit is described as following:

$$M_\pi = M_4 . M_3 . M_5 \tag{3.46}$$

where $M_3$is the series components and M_4 is the shunt components of the T-shaped structure that is seen in the figure 3.10 (b).

$$M_3 = \begin{bmatrix} \cos(\theta_3) & jZ_3 \sin(\theta_3) \\ jY_3 \sin(\theta_3) & \cos(\theta_3) \end{bmatrix} \tag{3.47}$$

$$M_4 = \begin{bmatrix} 1 & 0 \\ jY_4 \tan(\theta_4) & 1 \end{bmatrix} \tag{3.48}$$

Substituting the (3.45), (3.47) and (3.48) in to the (3.46)

$$\begin{bmatrix} 0 & jZ_0 \\ jY_0 & 0 \end{bmatrix} = \begin{bmatrix} 1 & 0 \\ jY_4 \tan(\theta_4) & 1 \end{bmatrix} \begin{bmatrix} \cos(\theta_3) & jZ_3 \sin(\theta_3) \\ jY_3 \sin(\theta_3) & \cos(\theta_3) \end{bmatrix} \begin{bmatrix} 1 & 0 \\ jY_4 \tan(\theta_4) & 1 \end{bmatrix} \tag{3.49}$$

After expanding equation 3.49, the term in the [ABCD] matrix can be written as

$$A = \cos\theta_3 - Z_3 Y_4 \sin\theta_3 \tan\theta_4 \tag{3.50}$$

$$B = jZ_3 \sin\theta_3 \tag{3.51}$$

$$C = jY_4 \sin\theta_3 \tan\theta_4 \left(1 - Z_3^2 Y_4^2 \tan^2\theta_4 + 2Z_3 Y_4 \tan\theta_4 \cot\theta_3\right) \quad (3.52)$$

$$D = \cos\theta_3 - Z_3 Y_4 \sin\theta_3 \tan\theta_4 \quad (3.53)$$

By evaluating the [ABCD] matrix, the following equations are obtained:

$$Z_3 = \frac{\sin\theta_3}{Z_0} \quad (3.54)$$

$$Z_4 = Z_3 . \frac{\tan\theta_4}{\cot\theta_3} \quad (3.55)$$

3.3.4 Meandering the Transmission Lines

In the microwave circuit design, the branchline couplers are generally designed with quarter wavelength transmission lines in the square or circular shaped dimensions [12]. However, there is a large unused blank chip area between the transmission lines. Since the conventional branchline couplers cover a large blank area, the cost of the device become expensive and also it is difficult for designers to integrate the conventional branchline coupler devices into the limited area of the microwave systems. Therefore, the designer wants to utilize the blank area between the transmission lines of the branchline coupler.

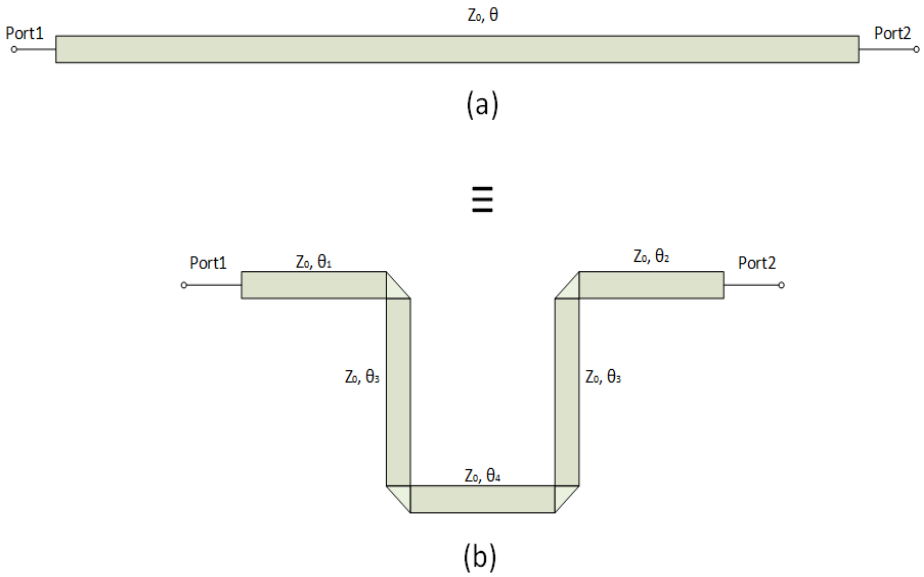

Figure 3.13: Meander Section

In the microwave design, the meandering of the transmission lines is a well-known and commonly used technique to reduce the size of the circuit. In this technique, the transmission lines are meandered into the blank area as seen in the figure 3.13. Each meandering section is consists of four bends. While each meandering sections is reducing the size of the branchline coupler, utilized bends in the meandered section add discontinuities. Furthermore, increasing the number of the meandering section means the decreasing the distances between the transmission line in the branchline coupler, and thigh meandering sections mean increasing the parasitic coupling between the transmission lines.

CHAPTER 4

MINIATURIZED BRANCHLINE COUPLER DESIGN FOR X-BAND APPLICATIONS

In this chapter, the miniaturized branchline coupler design is discussed according to the theoretical basis that is described in the previous chapters. The design goal of the branchline coupler is to miniaturize the conventional branchline coupler which operates in X band (8.5 – 10.5 GHz) and have a 90˚±5˚ phase difference between the two output ports with the operation frequency bandwidth as wide as possible. In this chapter, first of all the basic miniaturized branchline coupler design is constructed using the ideal transmission lines and ideal lumped elements and S-parameter simulations and optimizations are carried out in the Agilent's Advanced Design System (ADS). After the miniaturized branchline coupler design with ideal elements is completed with the lumped elements, simulations are continued on Agilent's Momentum (2.5D electromagnetic simulation tool of ADS). The transmission lines are realized with the coplanar waveguide guide (CPW) technology and lumped elements are replaced by distributed equivalents. The 2.5D electromagnetic simulations (EM) and optimizations were performed in the ADS Momentum. Finally, the completed miniaturized branchline coupler design was constructed in the Sonnet 3D electromagnetic simulator, the simulation results of both simulators are compared in terms of accuracy and time. The final version of the miniaturized branchline coupler is reshaped according to the feedback of the ADS Momentum and Sonnet EM simulations. In the following sections, the design process of the miniaturized branchline coupler is given step by step.

The miniaturization techniques in microwave applications are useful to reduce the size of the branchline coupler design, and to give opportunity to widen the operation bandwidth. In this thesis, two different miniaturized branchline coupler designs are realized, fabricated and measured. In the each miniaturized branchline coupler design, different miniaturization techniques are utilized, T-shape structures, π-shape structures and meandering the TL techniques, are utilized in order to miniaturize the conventional branchline coupler as small as possible.

In this chapter, two different mBLC designs will be given. In the first design, mBLC is consists of T-shape structures with open stubs and π-shape structures with open stubs and the TLs in both T-shape and π-shape structures were meandered. However, the sizes of the opens stubs, which were bended, limited the usage of the meandering transmission line techniques effectively. After the evaluation of the first mBLC, in the second design, open stubs were replaced with the MIM capacitors. In other words, the second mBLC design was constructed with T-shape structures with MIM capacitor, π-shape structures with MIM capacitors and TLs in the T-shape and π-shape structures were meandered. Therefore, the size of the second mBLC design is smaller than then the first mBLC design. The details of the two different mBLC designs are explained step by step in the following parts.

4.1 General Design Considerations of the Miniaturized Branchline Coupler

In this part, design of a miniaturized branchline coupler (mBLC) for X band applications with using the miniaturization techniques is presented. Due to the compactness and easiness to system integration requirements, the miniaturization techniques are taken into the consideration. In the design step, first the BLC design was started with using ADS ideal CPW transmission lines to make the simulations and optimizations in a short time. After that, the ideal CPW transmission lines were realized in the ADS Momentum and 2.5D EM simulations were performed. After that, the designed mBLCs were reconstructed in the Sonnet Suites and 3D EM

simulations were performed. Finally, the accuracy and simulation time duration of the ADS Momentum and Sonnet Suites were compared with reference to the measurement results.

4.1.1 mBLC Design with Using ADS CPW Tools

In this section, the design of the miniaturized branchline coupler will be explained step by step. Firstly, the sizes of the coplanar waveguide (CPW) transmission lines are determined for constructing the horizontal and vertical branches. In order to determine the width and slot of the each transmission line, the ADS linecalc utility is used to determine the impedances of the coplanar waveguide (CPW) transmission lines. After the sizes of the coplanar waveguide (CPW) transmission lines are chosen, the branchline coupler (BLC) is constructed with the ideal CPW transmission lines. In order to miniaturize the quarter wavelength coplanar waveguide (CPW) transmission lines, the π-shaped and T-shaped structures are utilized in the vertical and horizontal branches respectively. Since there is no tee or bend models for coplanar waveguide (CPW) technology in the Advanced Design System (ADS) design tool, these models are used from the Advanced Design System (ADS) microstrip design tool. In order to achieve the expected design performance of the branchline coupler, all the parameters of the coplanar waveguide (CPW) transmission lines are tuned manually. After the performance of the branchline coupler is in the vicinity of performance criteria all the parameters are subjected to optimization. In the parameter optimization, the limits of the parameters are chosen such that, fabrication of the BLC is in the fabrication limits of NANOTAM and unwanted coupling between the backside of the material and CPW lines are eliminated. Therefore, the ground-space ratio and the distances between the coplanar waveguide (CPW) transmission lines are controlled with the limitations in the optimization step.

The schematic of the miniaturized branchline coupler with using Advanced Design System (ADS) coplanar waveguide (CPW) tools is given in the figure 4.1. In this design, the quarter wave transmission line branches in horizontal arms are replaced by T-shape structures with parallel connected open stubs and quarter wave transmission line in vertical arms are replaced by π-shape structures with parallel connected open circuit stub. In additional to this, the isolation port is terminated with the ideal resistor which has a characteristic impedance of 50Ω.

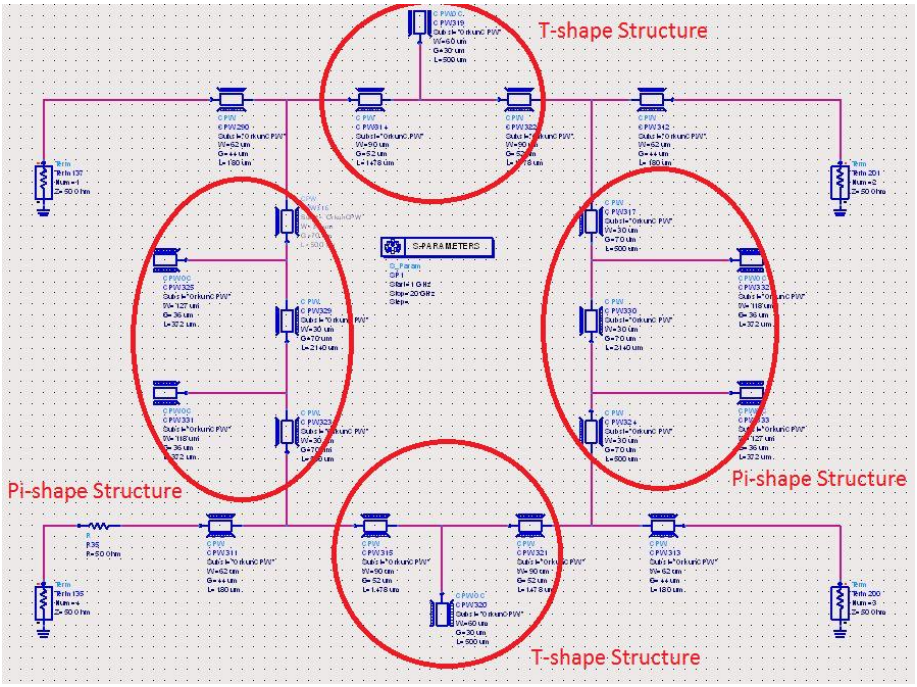

Figure 4.1: Schematic of the mBLC in ADS

In the design process, so as to miniaturize the BLC, the TLs were utilized as meander. Since there is no CPW bend or tee model in the ADS design tool, the microstrip models are utilized to add the discontinuities into the S-parameter simulations. In each meandering section, there are four bends and each bend gives discontinuities to the design. In order not to take the electromagnetic coupling of the transmission lines, in the design the distances between the transmission lines in the

meandering section were taken into the consideration. The completed design schematic of the first miniaturized branchline coupler design is illustrated in the Figure 4.2.

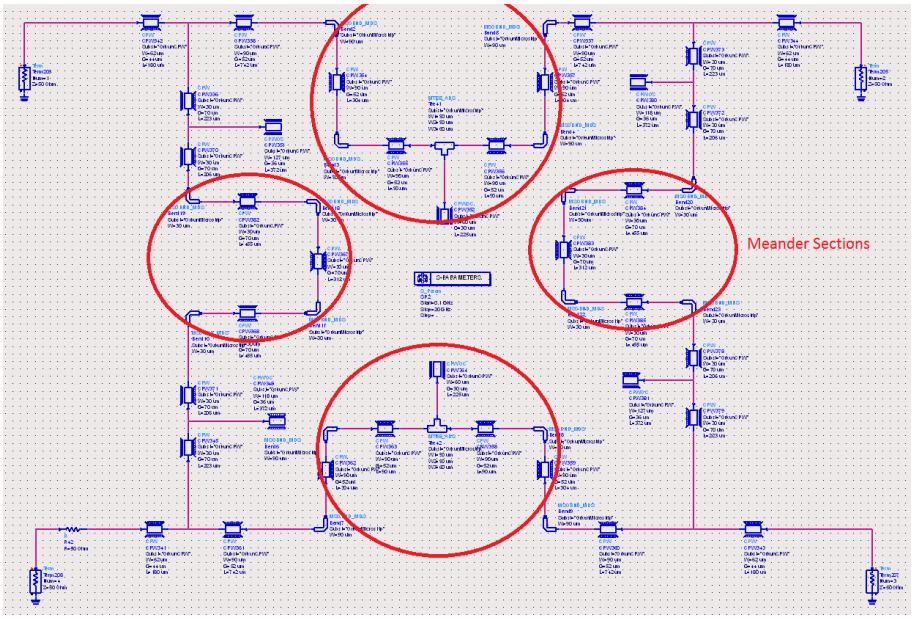

Figure 4.2: Schematic of the mBLC with Meander Sections in ADS

After the design step is completed, the performance of the miniaturized branchline coupler is determined with S-parameter simulations. So as to obtain the performance of the miniaturized branchline coupler, the S-parameter simulations are done in the frequency range of DC to 20GHz. In order to simulate the constructed design with using ADS CPW design tool, firstly the substrate parameters of the ADS CPW and microstrip design tools are adjusted, according to the fabrication parameters. The design is growth on a 300 nm SiC substrate which has a relative permittivity of 9.8. In additional to this, the metal thickness of the CPW transmission lines is taken as 2.5um and the conductivity is taken as 3e7 S/m. The substrate properties of the CPW and microstrip technologies are given as the Figure 4.3.

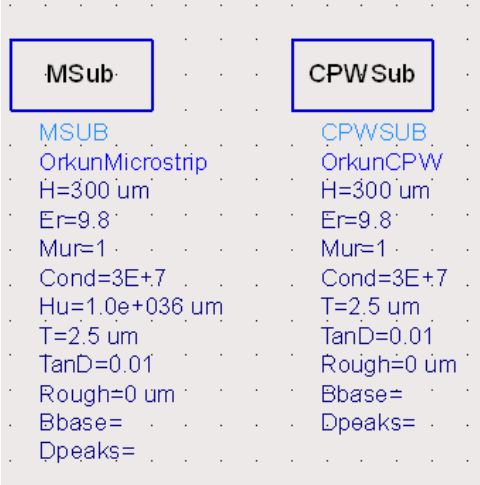

Figure 4.3: Substrate Parameters

Figure 4.4 shows the reflection coefficients of the each four ports at the frequency range of DC to 20GHz. As a design criteria, it was chosen that for the operation bandwidth return loss should be less than -10 dB and phase difference between the output ports is 90˚± 5˚. It was seen that, return losses of all ports are better than -10 dB in the frequency range of 8.5 to 10.5GHz.

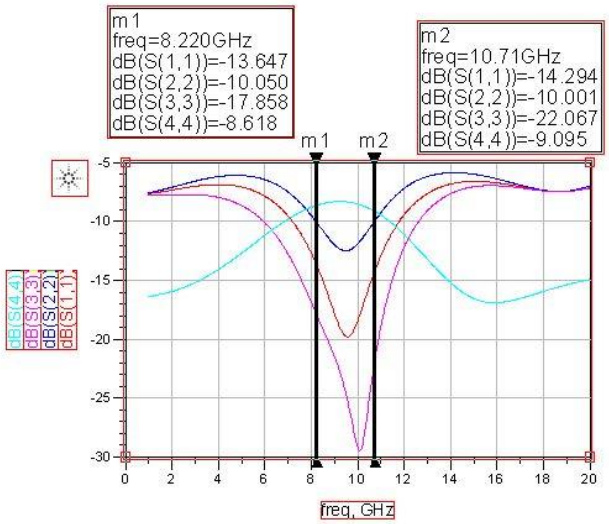

Figure 4.4: S-parameter Simulation Results of the mBLC with ideal CPW TLs in ADS

Figure 4.5 shows the through and coupled transmission of the miniaturized branchline coupler. In the simulations, it was seen that the through and coupled transmission are better than -3.6dB with the ideal ADS CPW transmission lines.

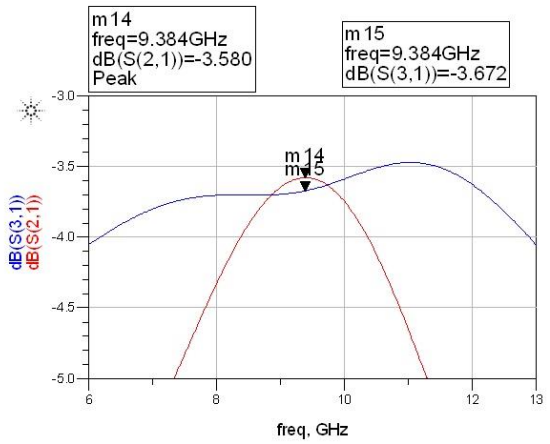

Figure 4.5: Direct (S21) and Coupled (S31) Port Transmission of the mBLC with ideal CPW TLs in ADS

The frequency response of the phase difference between the coupled and through ports is illustrated in the Figure 4.6. At the center frequency, it is shown that the 90˚ phase difference was achieved and in the operation frequency bandwidth the ripple of the phase difference is better than 5 ˚.

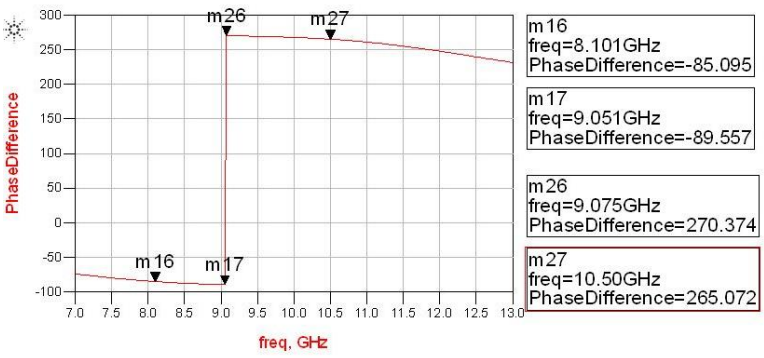

Figure 4.6: Phase Difference Between the Output Ports of mBLC with ideal CPW TLs in ADS

4.2 Design of Miniaturized Branchline Coupler in ADS Momentum

In this section, design and simulation of the miniaturized branchline coupler with utilizing the Agilent's ADS Momentum is presented. In this work, two different mBLC designs were realized in the ADS Momentum. Due to the ADS Momentum's 2.5D modeling capability that includes the coupling through the substrate and between the metal layers, it is decided to utilize the Agilent's ADS Momentum 2.5D EM simulator in the miniaturized branchline coupler design. Moreover, the ADS Momentum is a method of moment (MoM) based a 2.5D EM simulator which is commonly used to design and simulate the multilayered media such as antennas, filters and via holes [10] and preferred especially for MMIC design where the main coupling is through the substrate.

BLC is consists of a variety of components (i.e. transmission lines, air bridges, capacitors) and each component has its own properties. In additional to this, each component in the design has to be defined with a different layer. Since ADS Momentum is mostly used in multilayer PCB design, CMOS design. In the ADS Momentum, each layer is defined with a variety of names and fabrication parameters. Furthermore, it is crucial to implement the fabrication parameters into the simulation parameters accurately; so as to obtain an accurate simulation results. In the figure 4.7 the layer definitions of the miniaturized branchline coupler is illustrated.

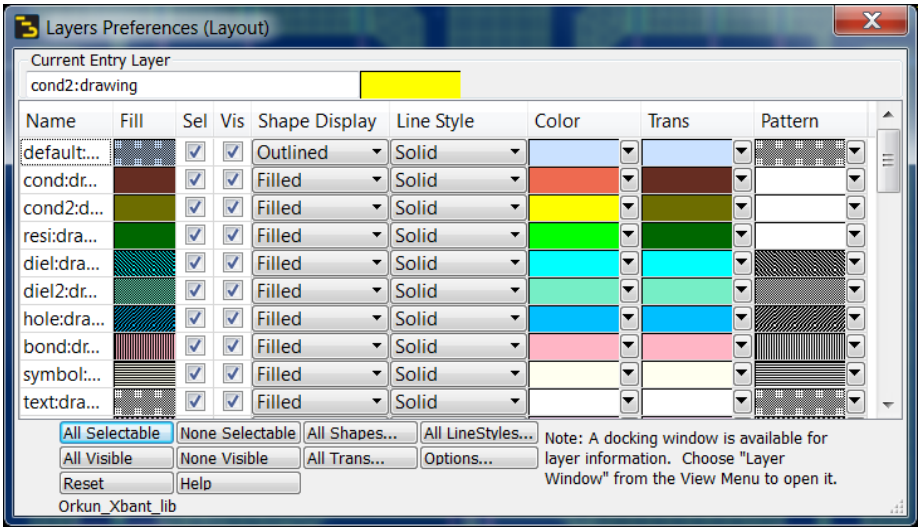

Figure 4.7: Layer Definitions of ADS Momentum

The next step in the design is to specify the substrate properties of the miniaturized branchline coupler. Layer stacking, layer thickness and electromagnetic properties of the layers should be defined accurately. All the parameters are defined according to the fabrication steps of NANOTAM. In the substrate properties, the gray color represents the conducting planes and the yellow color represents the conducting metals. Moreover, the blue color represents the dielectric media between the conducting planes (i.e. air, SiN). In the design, "cond" layer is defined for the metal-1 (i.e. underpass, MIM capacitor), "cond2" layer is defined for the metal-2 (i.e. transmission lines, grounds), the "resi" layer is defined for the air bridges (the bridges that connects the cond-1 layers to each other (i.e., transmission lines passes over the cond layer using this layer), and "symbol" layer is defined for the resistor and resistivity is defined for this layer. In additional to this, "bond" and "diel" are the conducting layers, which connects cond-1 layer to cond layer and defined as via. The design is fabricated on a 300um Silicon Carbide (SiC) wafer and there is 300nm silicon nitride (SiN) passivation on the top of the both layers of "cond" and "symbol", this layer also serves as the dielectric layer of MIM capacitors. Furthermore, 3.5um air is defined between the layers "resi" and "cond2"; because of having 3.5um height in the air bridge topology in NANOTAM's fabrication process

and the metal thickness is taken as 2.5um for “cond2”. Finally, the entare substrate that is used in the ADS Momentum is illustrated as in the figure 4.8.

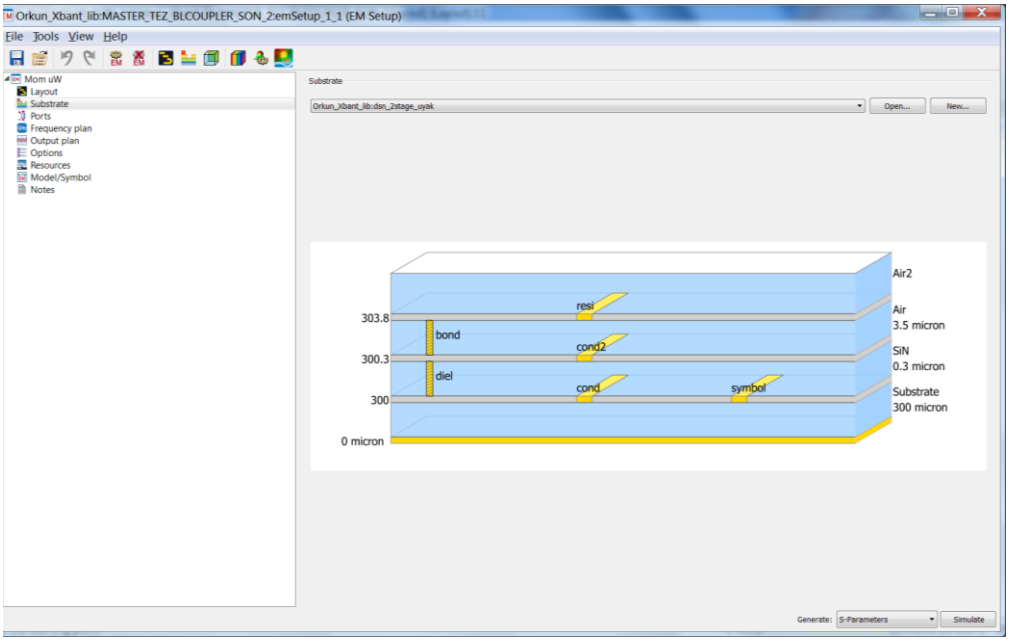

Figure 4.8: Substrate Definition of ADS Momentum

After that, 2-D layout of the miniaturized branchline coupler, which is designed in the previous section, is drawn according to the specified layer and substrate definitions. In this design, the ground planes are connected to each other with the underpass metals (i.e., using cond layer) and transmission lines that are cond-1 layer pass over this underpasses metals via the air bridges (resi layer). The reason that the air bridges are utilized in the design is that “In the CPW two fundamental modes are supported: the coplanar mode, and the parasitic slotline mode. Air bridges between ground planes have to be applied to suppress the undesired slotline mode. These air bridges must be located at short intervals (less than $\lambda_g/4$ apart). “[11]. The air bridge structure is design in the ADS Momentum as seen in the figure 4.9.

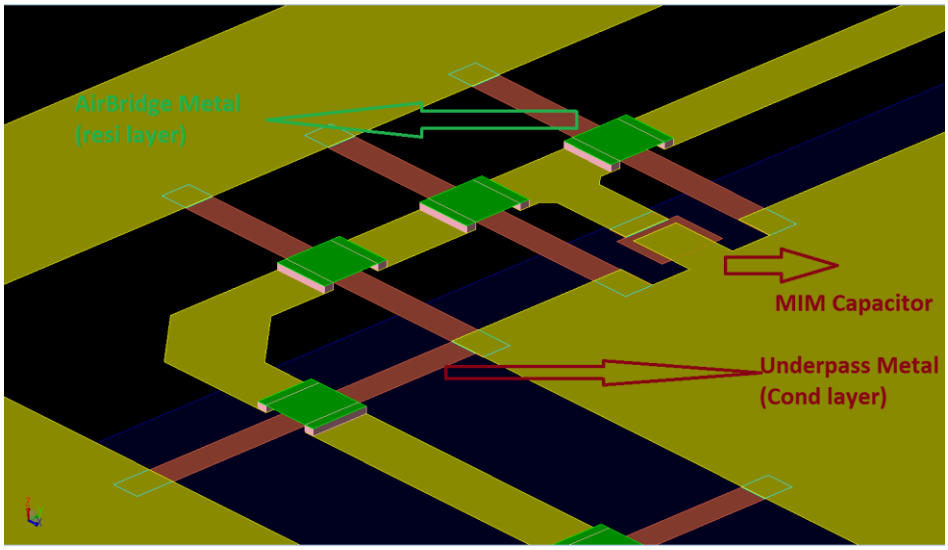

Figure 4.9: Air Bridge Design in ADS Momentum

4.2.1 The first mBLC Design in ADS Momentum

In this subsection, the first mBLC design was done with using the miniaturization techniques which were discussed as in the figure 4.10. In the design, firstly 2D layout of the first miniaturized branchline coupler is drawn according to the theoretical bases and simulation results with ADS ideal CPW elements. In order to reduce the parasitic effects and prevent the ground problem, the air bridge and underpass structures were drawn in the layout. In additional to this, the isolation port was terminated with the characteristic impedance of 50Ω internally. The completed first mBLC design has miniaturized to the sizes of 2320x1970um and 55% size reduction was achieved with reference to conventional BLC. Figure 4.10 shows the 2D layout and 3D view of the first mBLC in ADS Momentum.

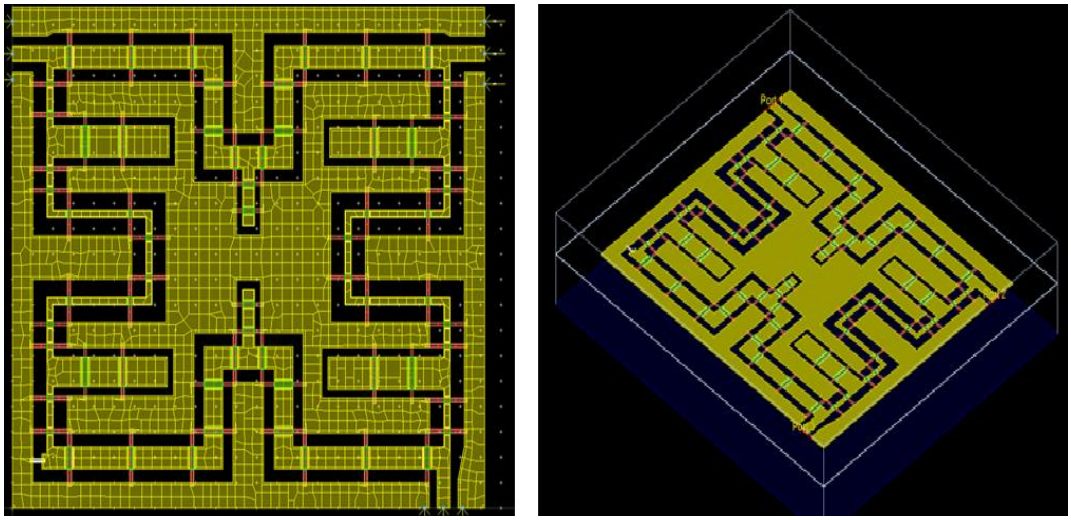

Figure 4.10: Layout and its 3-D view of the first mBLC in ADS Momentum

4.2.2 The second mBLC Design in ADS Momentum

In the second miniaturized branchline coupler design, all the design steps were repeated and in the miniaturization techniques, quarter wavelength TLs were replaced with T-shape structures with parallel connected MIM capacitor, π-shape structures with MIM capacitors. Moreover, in the second mBLC design, TLs in the T-shape and π-shape structures were meandered. In the second mBLC design, the usage of the MIM capacitor instead of utilizing the open stubs, give opportunity to increase the lengths of the meandering sections and the size of the miniaturized branchline coupler become smaller. Therefore, in the second mBLC, the area of the mBLC was less than the first mBLC design. The completed second mBLC design has the sizes of 1950x2000um and 62% size reduction was achieved with reference to conventional BLC. Figure 4.11 shows 2D layout and 3D view of the second mBLC design.

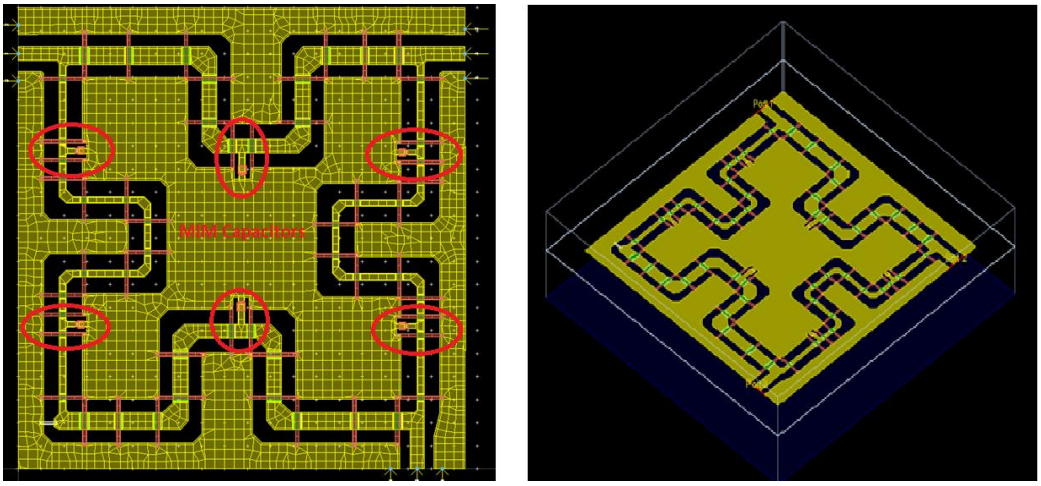

Figure 4.11: 2D Layout and its 3-D view in ADS Momentum for the second mBLC

4.3 Simulation Results of the mBLC Designs in ADS Momentum

In this section, the EM simulations results of the mBLC designs were presented. In the previous subsections two different mBLC designs were done in ADS Momentum. In order to, simulate the mBLC design, first port and reference ground definitions were specified for each port. In additional to this, the reference impedances of the common ports are set to the 50Ω. The port definition is illustrated in the figure 4.12.

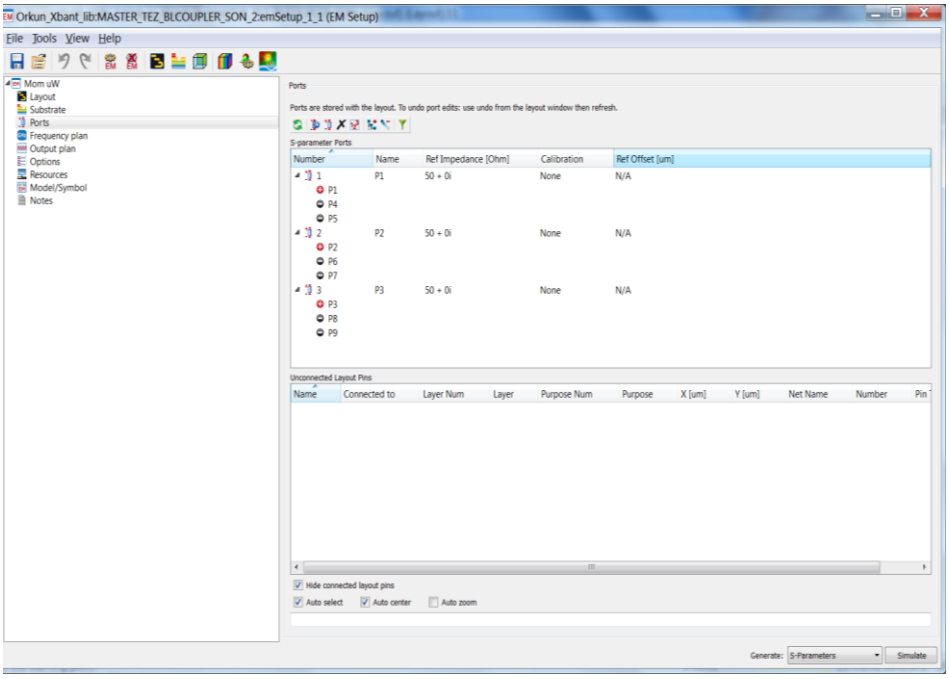

Figure 4.12: Port Definitions of ADS Momentum

The next step in the simulation process is to set the mesh options. In the EM simulations, mesh property is a very crucial issue which directly affects the accuracy of the simulations and simulation time. In the EM simulations, the density of mesh in the simulations should be high in order to obtain accurate results; but too high values may result in very high simulation times. Moreover, in the EM simulation all of the characteristic properties of the circuit geometry, including edge effect, metal thickness, etc, have to be taken into the calculation; and this can be achieved by increasing the mesh density of the EM simulation to sufficiently high values. On the contrary, increasing the mesh density increases the simulation duration and sometimes simulators waste too much time on the unnecessary details. Therefore, in the mesh property, the mesh density of the EM simulation is chosen as the 120cells/wavelength and the mesh frequency is chosen as the highest simulation frequency. The mesh property of the EM simulation is given in the figure 4.13.

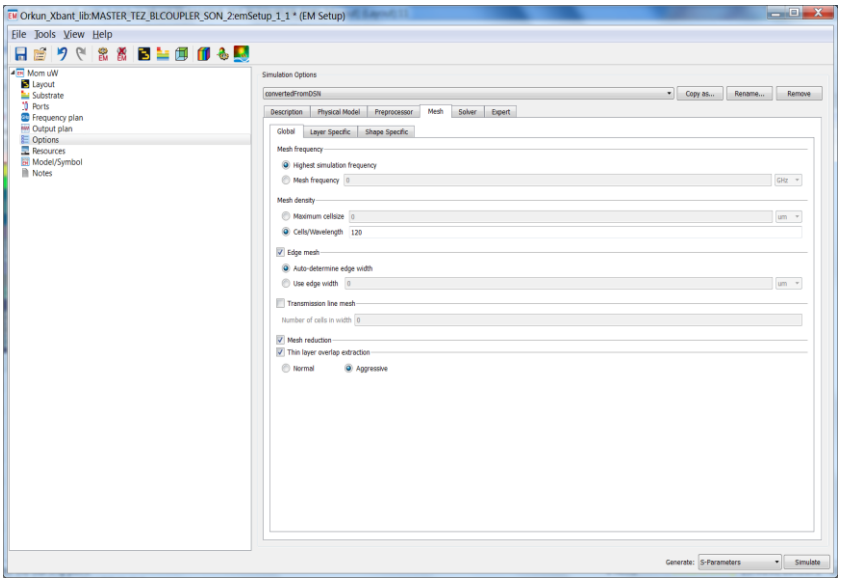

Figure 4.13: Mesh Property of ADS Momentum

Finally, the frequency plan of the EM simulation is chosen from DC to 30 GHz, as well as the number of the points is chosen as 501 as seen in the figure 4.14.

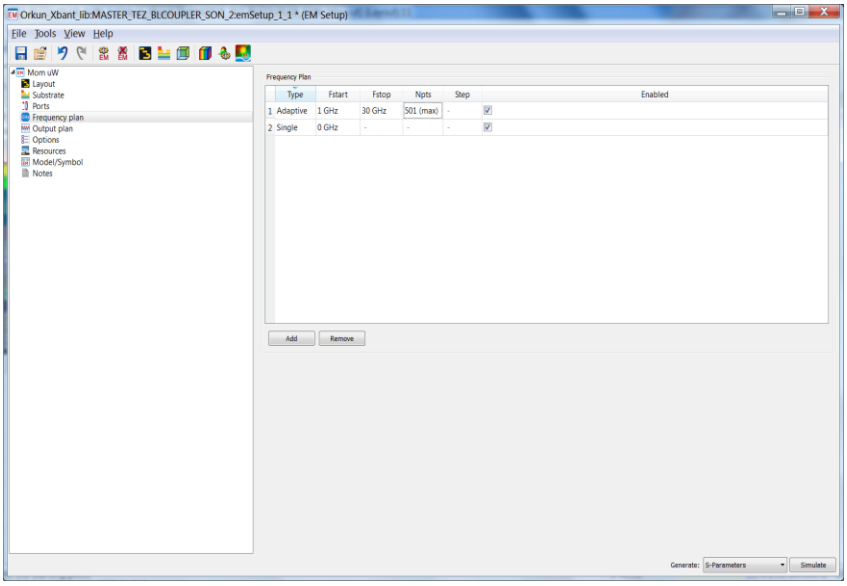

Figure 4.14: Frequency Plan of ADS Momentum

4.3.1. Simulation Results of first mBLC Design in ADS Momentum

Figure 4.15 shows the s-parameter simulation results of the first mBLC design. According to the ADS Momentum 2.5D EM simulation results, the reflections of the input and output ports are better than -10dB and the isolation between the input port and the isolation port is better than -10dB in the operation frequency bandwidth (8.5-10.5 GHz). In additional to this, the through and coupled port transmission losses are around 3.6dB, as well as the phase difference between the through and coupled ports are 90˚±5˚. Moreover, the current density of the mBLC for the first design is given in the figure 4.16.

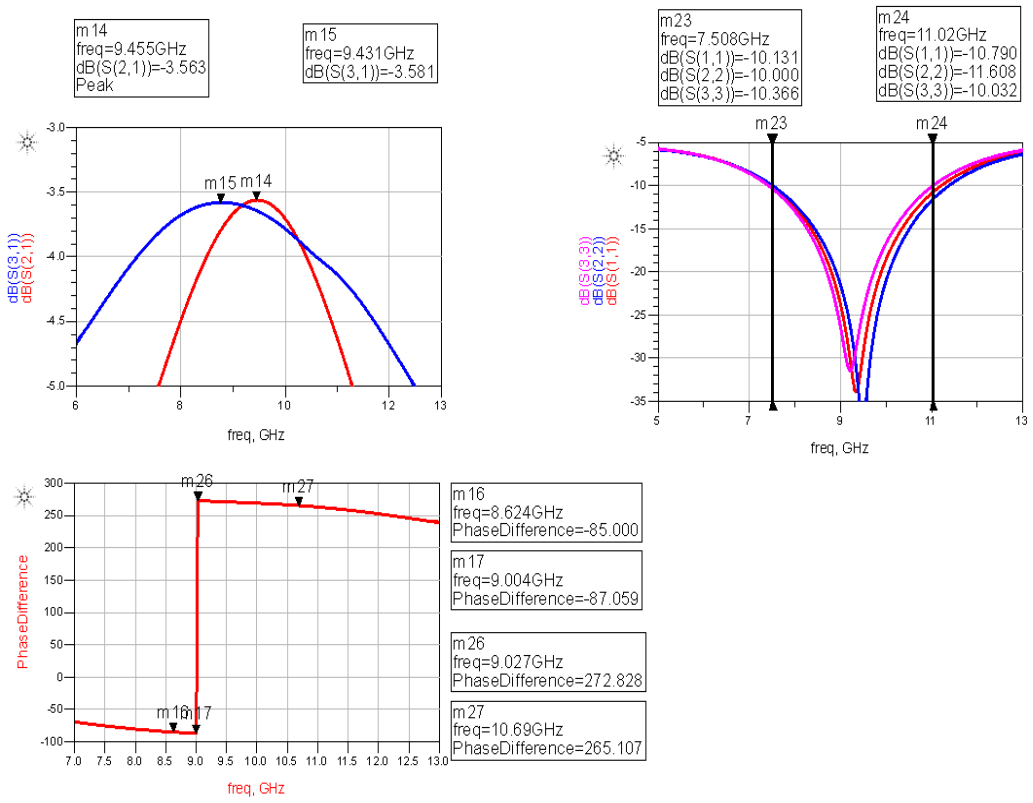

Figure 4.15: EM Simulation Results (ADS Momentum) of mBLC for the first design a) Input/Output Reflections b) Through (S21) and Coupled (S31) Port Transmission c) Phase Difference between the Output Ports

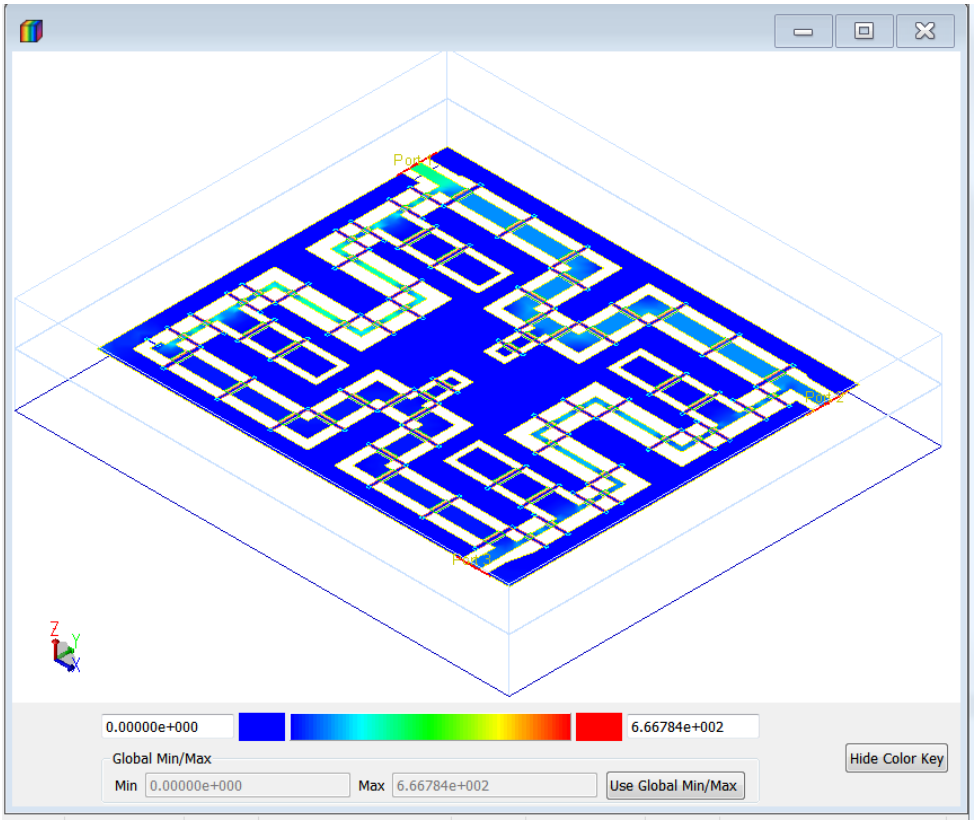

Figure 4.16: Volume Current Density of the mBLC for the first design

4.3.2 Simulation Results of second mBLC Design in ADS Momentum

Figure 4.17 shows the s-parameter simulation results of the second mBLC design. According to the ADS Momentum 2.5D EM simulation results, the reflections of the input and output ports are better than -10dB and the isolation between the input port and the isolation port is better than -10dB in the operation frequency bandwidth (8.5-10.5 GHz). In additional to this, the through and coupled port transmission losses are around 3.6dB, as well as the phase difference between the through and coupled ports are 90˚±5˚. Furthermore, the current density of the mBLC for the second design is illustrated in the figure 4.18.

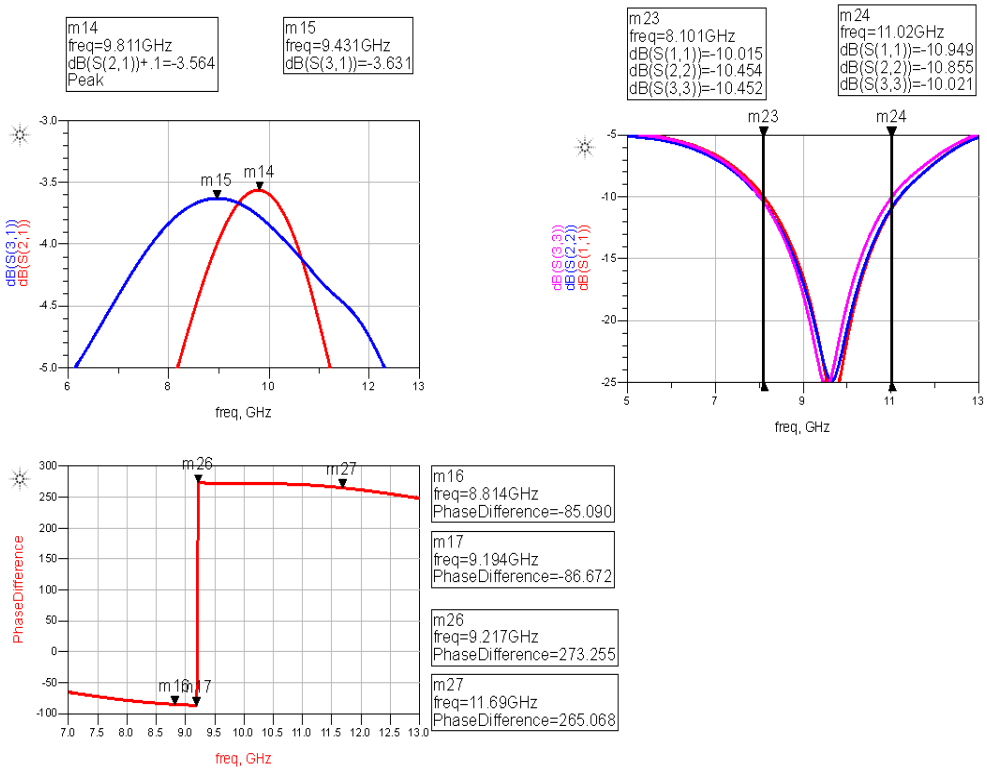

Figure 4.17: EM Simulation Results (ADS Momentum) of mBLC for the second design a) Input/Output Reflections b) Through (S21) and Coupled (S31) Port Transmission c) Phase Difference between the output ports

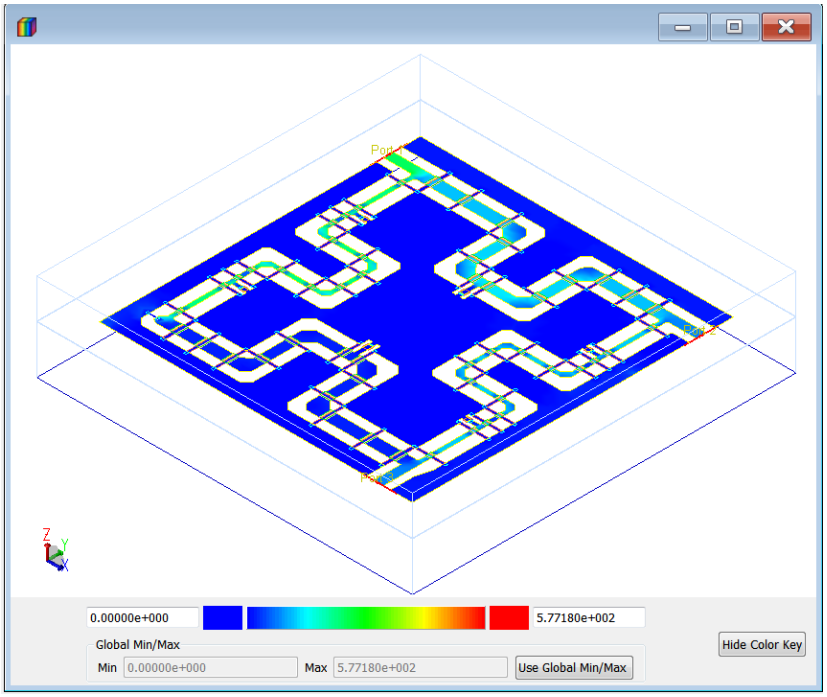

Figure 4.18: The Volume Current Density of the mBLC for the second Design

4.4 Design of the Miniaturized Branchline Couplers in Sonnet Suites

In this section, design and simulation of the miniaturized branchline coupler (mBLC) designs with utilizing the Sonnet Suites are presented. Due to the high accuracy and reliability benefits of the Sonnet Suites, it was decided to simulate mBLC designs with utilizing Sonnet Suites 3-D electromagnetic (EM) simulator. "Sonnet Suites is a 3-D electromagnetic (EM) simulator which is utilizing a rigorous Method-of-Moment EM analysis based on Maxwell's equations that includes all parasitic, cross coupling, enclosure and package resonance affects." [8].

In the Sonnet Suites, first of all the dielectric layers are defined, so as to construct the multilayered mBLC designs. In order to construct the mBLC, 5 different layers are specified which are listed from bottom to top as named Air, Gallium Nitride (GaN), Silicon Nitride (SiN), Air Bridge and Air.

In the ADS Momentum, each layer is defined with a different variety of names and fabrication parameters. Furthermore, it is crucial to specify the fabrication parameters accurately; so as to obtain an accurate simulation results. In the figur3.6 the layer definitions of the miniaturized branchline coupler is illustrated. In the dielectric layer definitions, the dielectric constant of the Silicon Carbide (SiC) substrate and Silicon Nitride (SiN) passivation layer are set to 9.8 and 7.5 respectively. In additional to this, the thickness of Silicon Carbide (SiC) substrate and Silicon Nitride (SiN) passivation layer are set to 300um and 0.3um. Moreover, the height of the air bridge structure is set as 3.5um according to the manufacturing parameter. Figure 4.19 shows the dielectric layers of the mBLC in the Sonnet Suites.

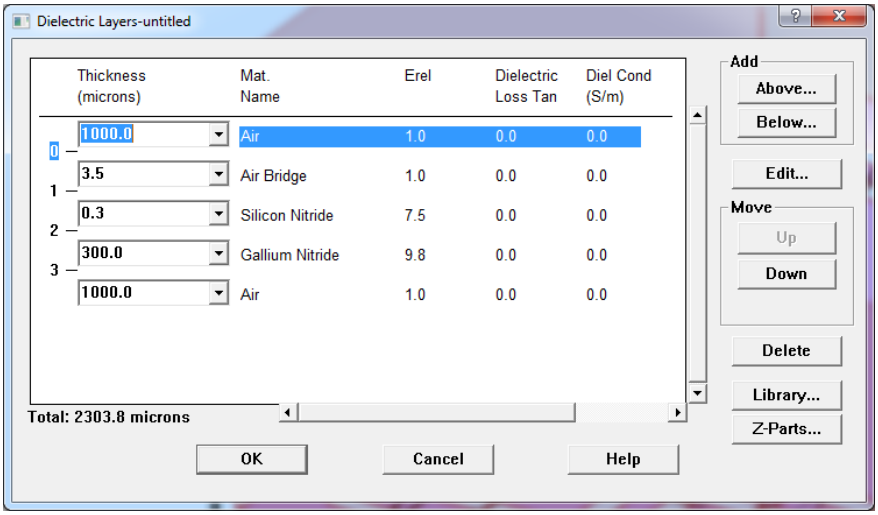

Figure 4.19: Dielectric Layers of the mBLC in the Sonnet Suites

The next step, in the design is to set the used metal types and parameter in the mBLC designs. In the design, four different types of metals were utilized. The utilized metals were specified as Gold1, Gold2, resist and via. “Gold1” metal was utilized to construct the underpass structures so as to connect the ground planes with each other (same as cond layer in ADS Momentum, figure 4.9). In additional to this, “Gold2” metal was utilized to construct the transmission lines and ground planes (same as cond2 layer in ADS Momentum, figure 4.9). Moreover, “resist” metal was utilized to construct resistor which was utilized to internally terminate the isolation port.

Finally, “via” metal was utilized to construct the foot of the air bridge structures and connections between “Gold1” and “Gold2” (same as bond layer in ADS Momentum, figure 4.9). Figure 4.20 shows the metal types of the mBLC designs in the Sonnet Suites.

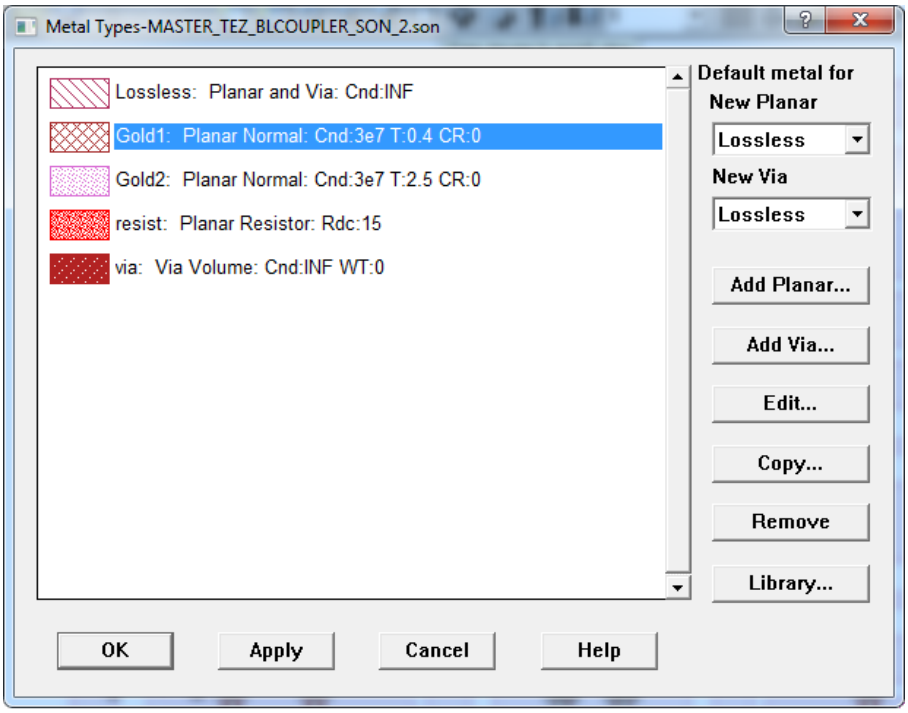

Figure 4.20: Metal Types of the mBLC in the Sonnet Suites

After the layer definitions and metal types of the mBLC designs are set, and then the 2-D layouts of the mBLC were drawn in the Sonnet Suites. In order to simplify the 2-D layout drawings, the mBLC designs are exported from the ADS Momentum as a gds file, then the layer definitions and metal types of the designs have rearranged according to the design parameters of the Sonnet Suites. In the design, the air bridges were design in the same locations as designed in the ADS Momentum and ground planes were connected with the underpasses and the transmission lines pass the underpass metal with using the air bridges. The air bridge and underpass structures of the mBLC design in the Sonnet Suites are given in the figure 4.21 (for the 3D view of this structure in ADS Momentum see figure 4.9).

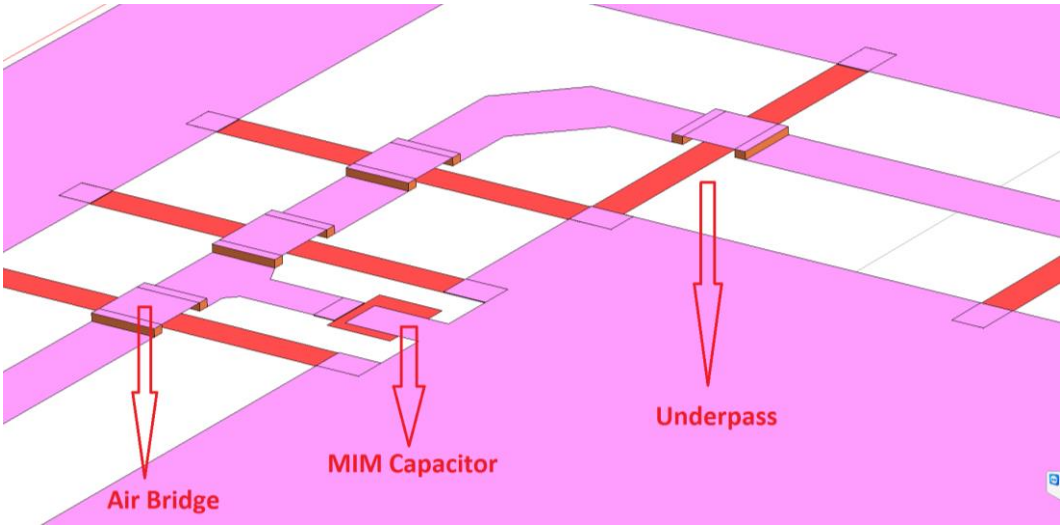

Figure 4.21: Air Bridge and Underpass Structures in the Sonnet Suite

4.4.1 The first mBLC design in Sonnet Suites

In the Sonnet Suites, the 2D layout of the first mBLC, which was designed in the ADS Momentum, was redrawn. In additional to this, the 3D EM simulation parameters of the Sonnet Suites were adjusted with respect to the fabrication parameters. Also, the properties of the first mBLC such as metal types, layer definitions etc. were specified as explained in the previous parts. Figure 4.22 shows the 2-D layout and 3-D view of the mBLC for the first design.

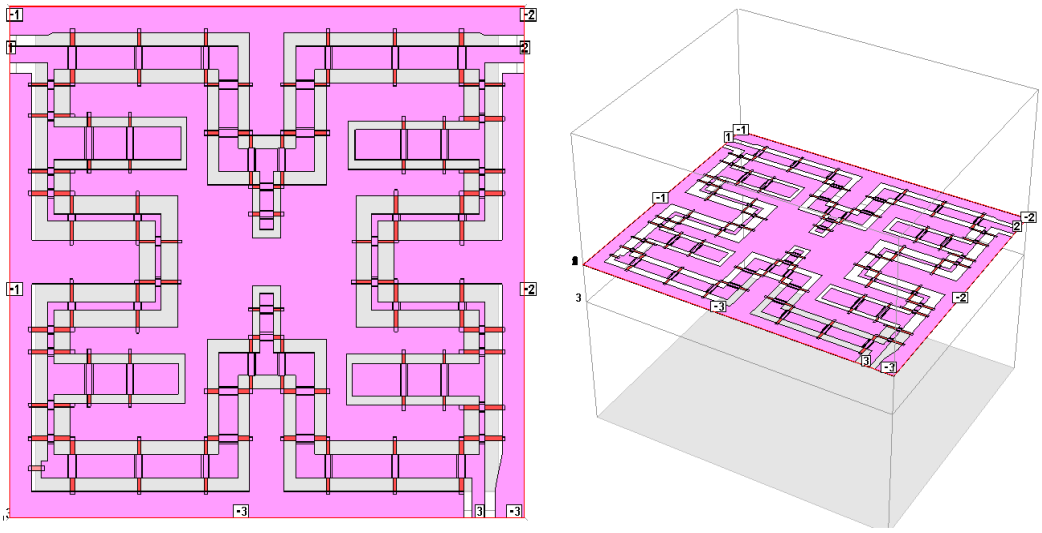

Figure 4.22: 2-D Layout and 3-D view of the mBLC for the first design in Sonnet Suites

4.4.2 The second mBLC design in Sonnet Suites

In the second mBLC design, all the design steps of Sonnet Suites were repeated. The ADS Momentum design was imported into the Sonnet Suites and the layer definitions and metal types were defined as mentioned in the section 4.4. The difference between the first mBLC is that the second mBLC design has MIM capacitors in the π-shaped and T-shaped structured miniaturization techniques. Figure 4.23 shows the 2-D layout and 3-D view of the mBLC for the second design in Sonnet Suites.

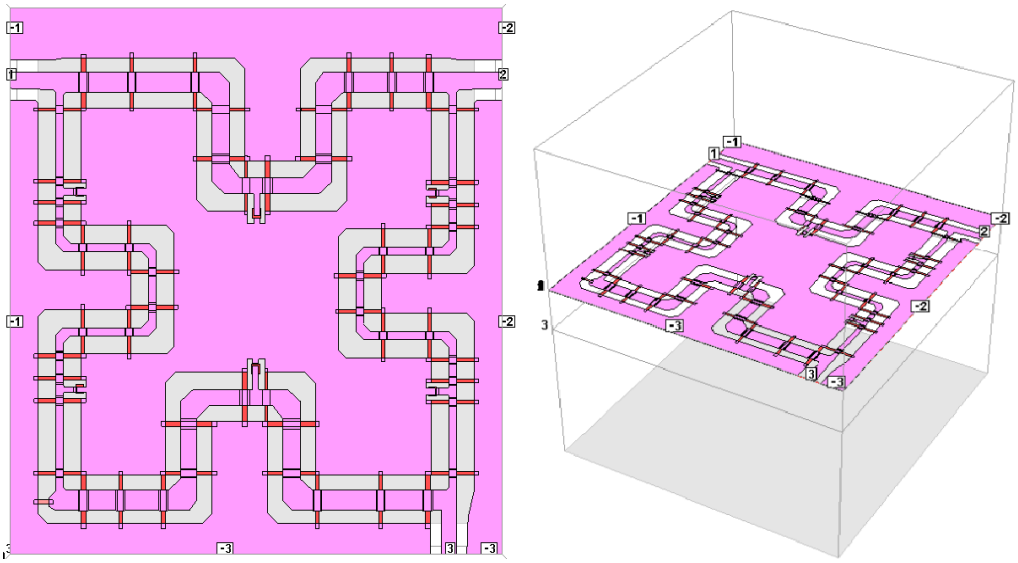

Figure 4.23: 2-D Layout and 3-D view of the mBLC for the second design in Sonnet Suites

The next step in the Sonnet Suites was to specify the port definitions. In the mBLC designs, there were four (4) ports and the isolation port was internally terminated with a 50Ω resistor. The other ports which are input, through and coupled ports were named as P1, P2 and P3 respectively and the ground reference planes were specified for each port. In additional to this, the ports were set to the characteristic impedance of 50Ω in the port definition. Figure 4.24 shows the port definition of the mBLC in the Sonnet Suites similar as defined in ADS Momentum (figure 4.12).

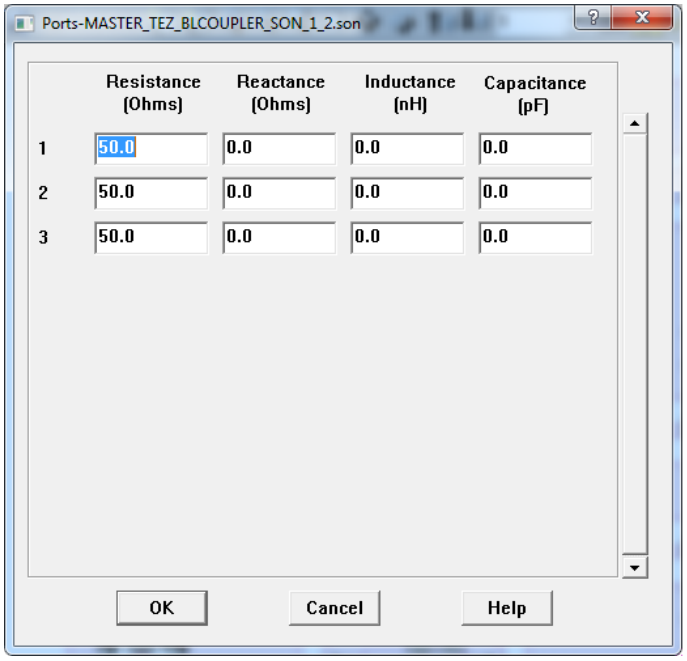

Figure 4.24: Ports of the mBLC in Sonnet Suites

In order to simulate the mBLC design in the Sonnet EM simulator, the mesh size of the EM simulation is determined with the cell size. In the EM simulation, the cell sizes were chosen as 4x4um because of optimizing the EM simulation duration and the accuracy of the simulations. The specified box sizes were taken equal to the sizes of the simulated mBLC design.

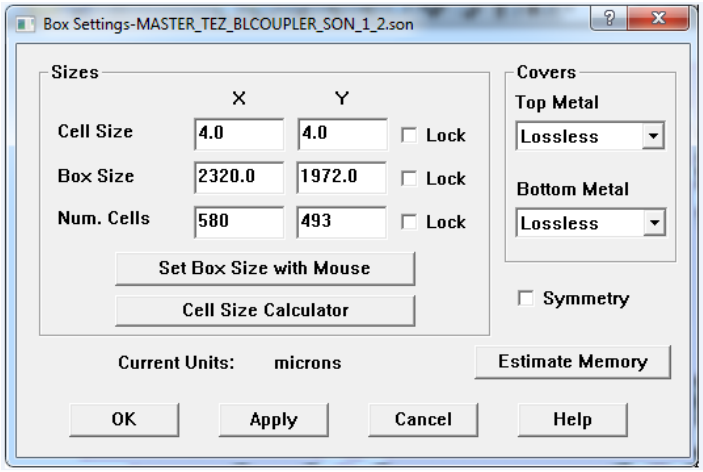

Figure 4.25: Box Settings of the mBLC in Sonnet Suites

Finally, the EM analysis setup is adjusted and the simulations were done in the frequency range of 1 to 20GHz. Figure 4.26 shows the analysis setup of the EM simulator in Sonnet Suites.

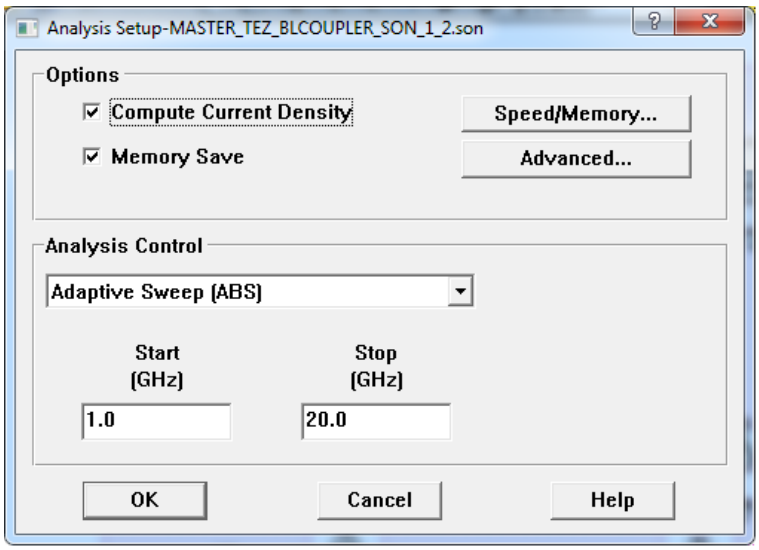

Figure 4.26: Analysis Settings of the mBLC in Sonnet Suites

4.5 Simulation Results of the mBLC Designs in Sonnet Suites

In this section, the EM simulations results of the mBLC designs with utilizing the Sonnet Suites are presented. The completed mBLC designs, which were discussed in the previous section, have simulated in the Sonnet Suites EM simulator.

4.5.1 Simulation Results of the first mBLC Designs in Sonnet Suites

Figure 4.27 shows the s-parameter simulation results of the first mBLC design. According to the Sonnet Suites 3D EM simulation results, the reflections of the input and output ports are better than -10dB and the isolation between the input port and the isolation port is better than -10dB in the operation frequency bandwidth (8.5-10.5 GHz). In additional to this, the through and coupled port transmission losses are around 3.7dB, as well as the phase difference between the through and coupled ports are 90˚±5˚. Moreover, in the current density of the mBLC for the first design is given in the figure 4.28.

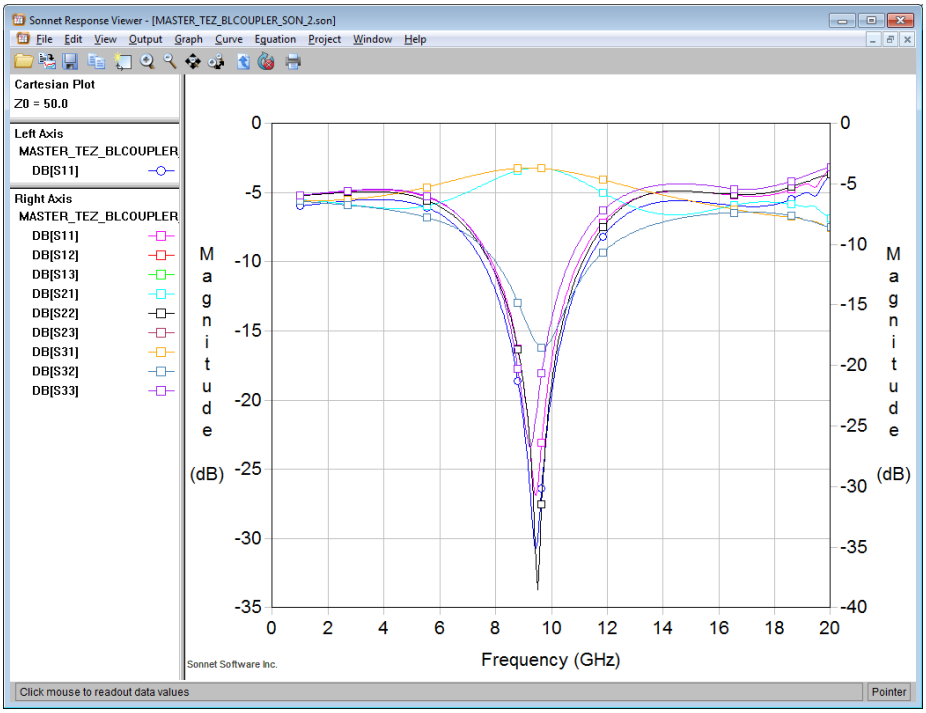

Figure 4.27: EM Simulation Results (Sonnet) of mBLC for the first design

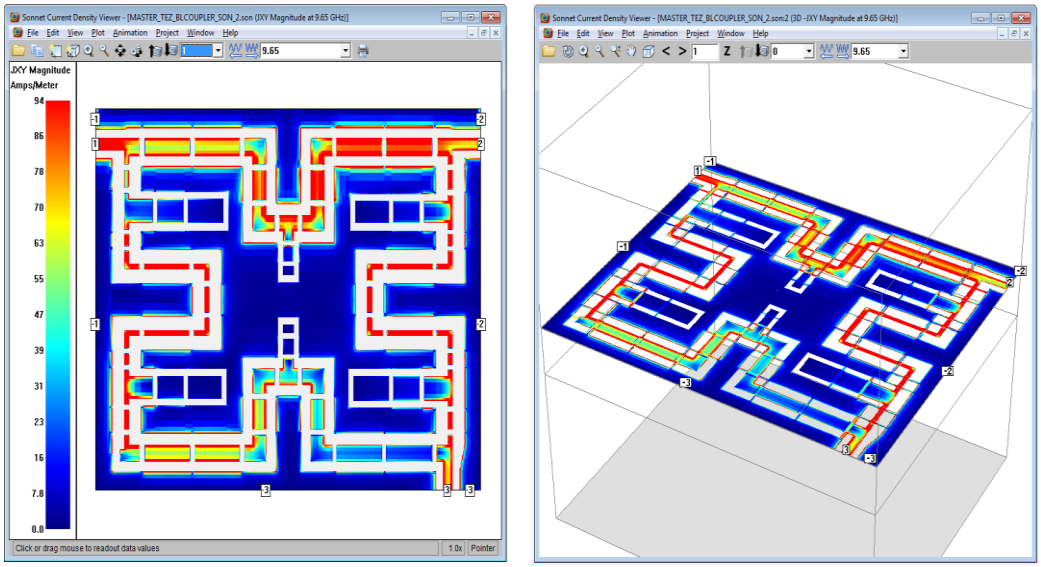

Figure 4.28: Current Density (Sonnet) of mBLC for the first design

4.5.2 Simulation Results of the second mBLC Designs in Sonnet Suites

Figure 4.29 shows the s-parameter simulation results of the second mBLC design. According to the Sonnet Suites EM simulation results, the reflections of the input and output ports are better than -10dB and the isolation between the input port and the isolation port is better than -10dB in the operation frequency bandwidth (8.5-10.5 GHz). In additional to this, the through and coupled port transmission losses are around 3.7dB, as well as the phase difference between the through and coupled ports are 90˚±5˚. Furthermore, the current density of the mBLC for the second design is illustrated in the figure 4.30.

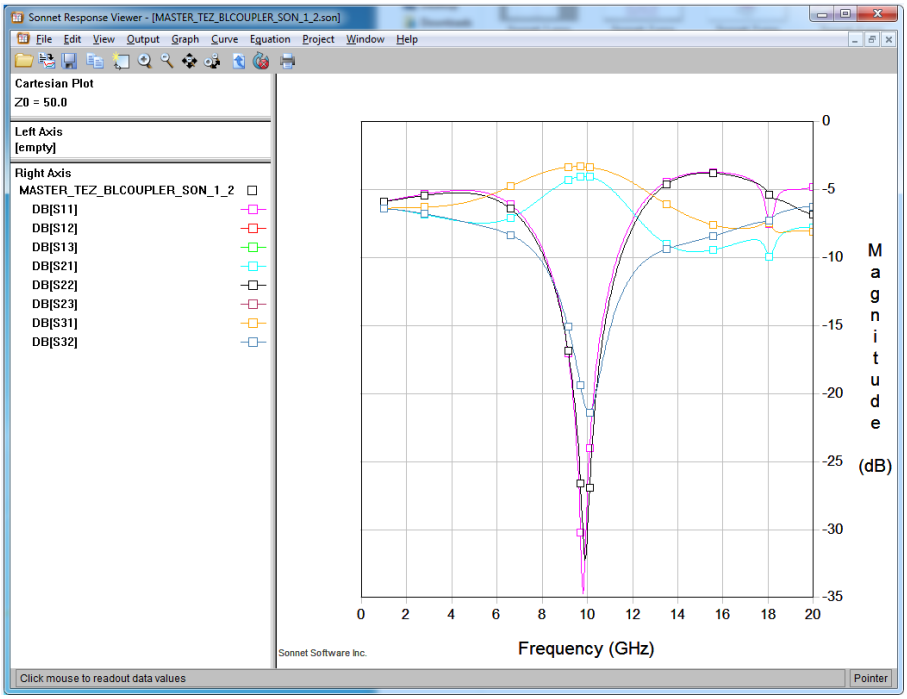

Figure 4.29: EM Simulation Results (Sonnet) of mBLC for the second design

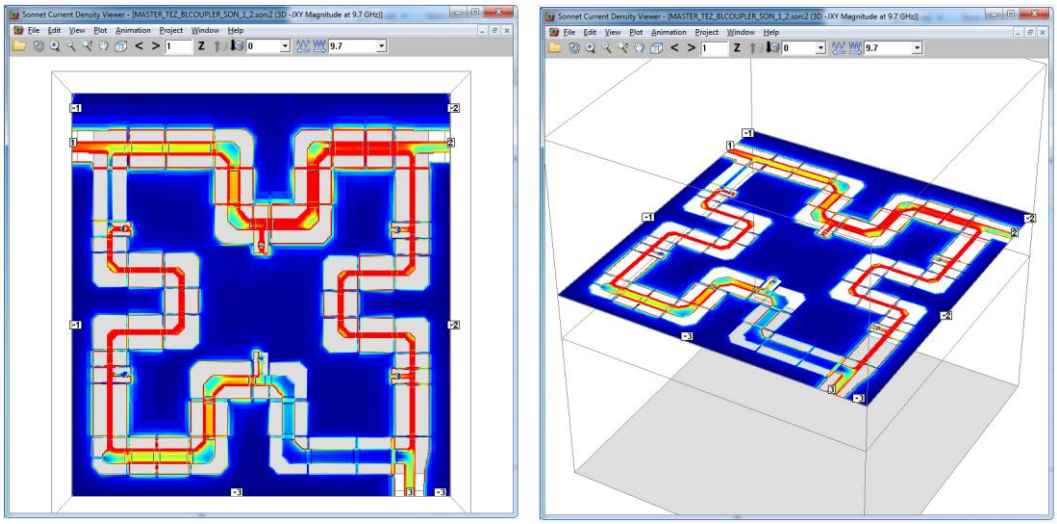

Figure 4.30: Current Density (Sonnet) of mBLC for the second design

In the Tablo 4.1, the obtained results and sizes of mBLC designs were compared with reference to the conventional branchline coupler (BLC). According to the EM simulation results, the sizes of the mBLCs were significantly reduced while other performance parameters were approxiametely same with the performance of the conventional BLC. In this table, bandwidth is calculated as the frequency range where return loss is less than -10dB and the phase difference between the two output ports is $90^{\circ} \pm 5^{\circ}$.

Tablo 4.1: The Comparisons between Conventional BLC and mBLC designs

	Conventional BLC	**First mBLC Design**	**Second mBLC Design**
Sizes	3200umX3200um	1970umX2320um	1950umX2000um
Size Reduction	-	55%	62%
Bandwidth	20.8%	21.9%	22.2%
Input/Output Return Losses	< -10dB	< -10dB	< -10dB
Phase Difference	90˚± 5 ˚	90˚± 5 ˚	90˚± 5 ˚

4.6 Photomask Design

In this subsection, the layouts of the designed mBLCs were redrawn according to photomask design rules. The photomask is an opaque plate which is a crucial component in manufacturing semiconductors [22]. In the photomask, each of the utilized layers and other fabrication steps were included. In order to design the photomask, first of all layouts of each active and passive devices were redrawn with specific photomask rules. The figure 4.31 show the layout of the photomask design which consists of designed mBLCs and test elements. After the photomask design was completed, the fabrication process with utilizing the photomask was started in Bilkent University Nanotechnology (NANOTAM) laboratories.

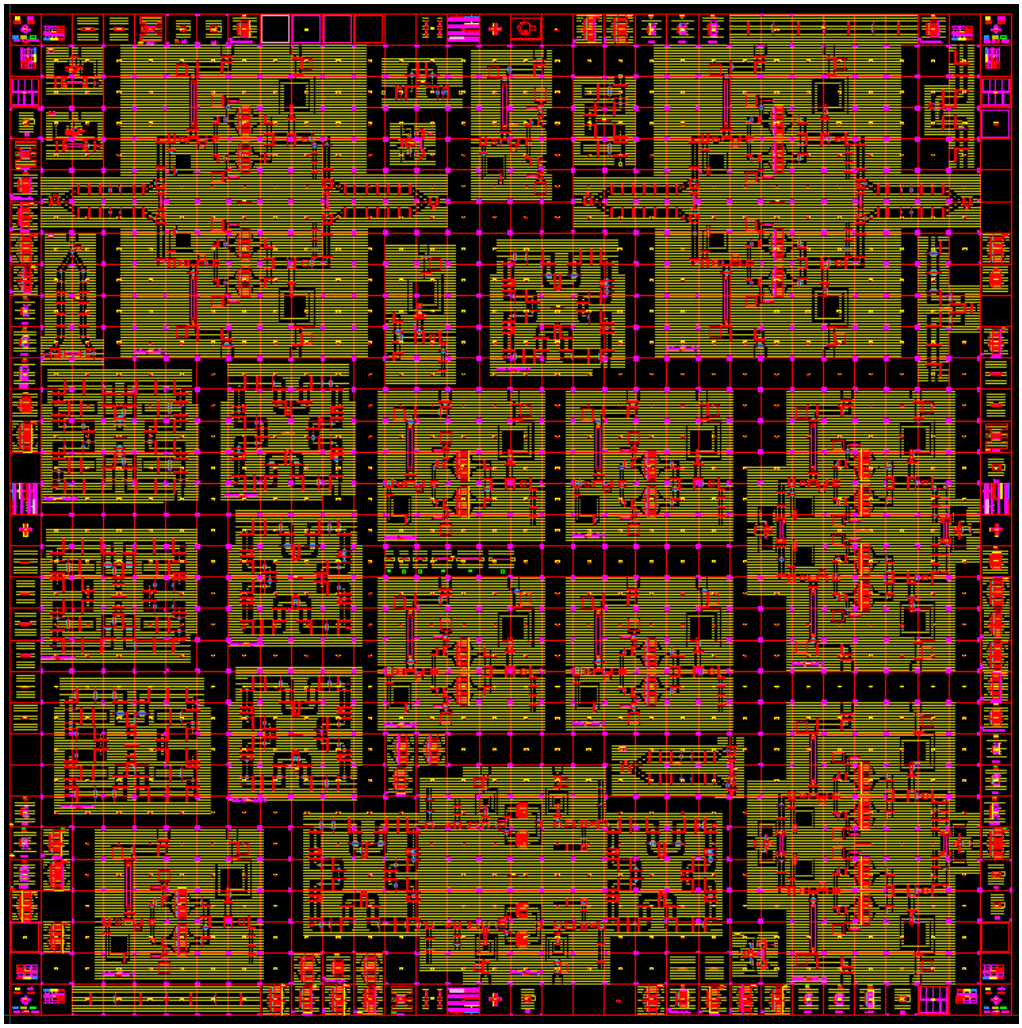

Figure 4.31: Photomask Design including mBLCs

CHAPTER 5

MEASUREMENT RESULTS

In this chapter, the fabricated miniaturized branchline coupler will be measured and the performance of the design with respect to simulation results will be discussed. In additional to this, the S-parameter measurement setup will be described and measurement techniques will be explained. Finally, the EM simulation results of ADS Momentum and Sonnet Suites will be compared with the measurement results.

5.1 S-Parameter Measurements

In this subsection, the S-parameter measurements details of the fabricated mBLCs were given. In order to analyze the performance of the fabricated mBLCs, the S-parameter measurement setup was utilized. The S-parameter measurement setup consists of Agilent E8361C (10MHz – 67GHz) network analyzer, Cascade M150 probe station and picoprobes. Figure 5.1 illustrates the photo of S-parameter measurement setup.

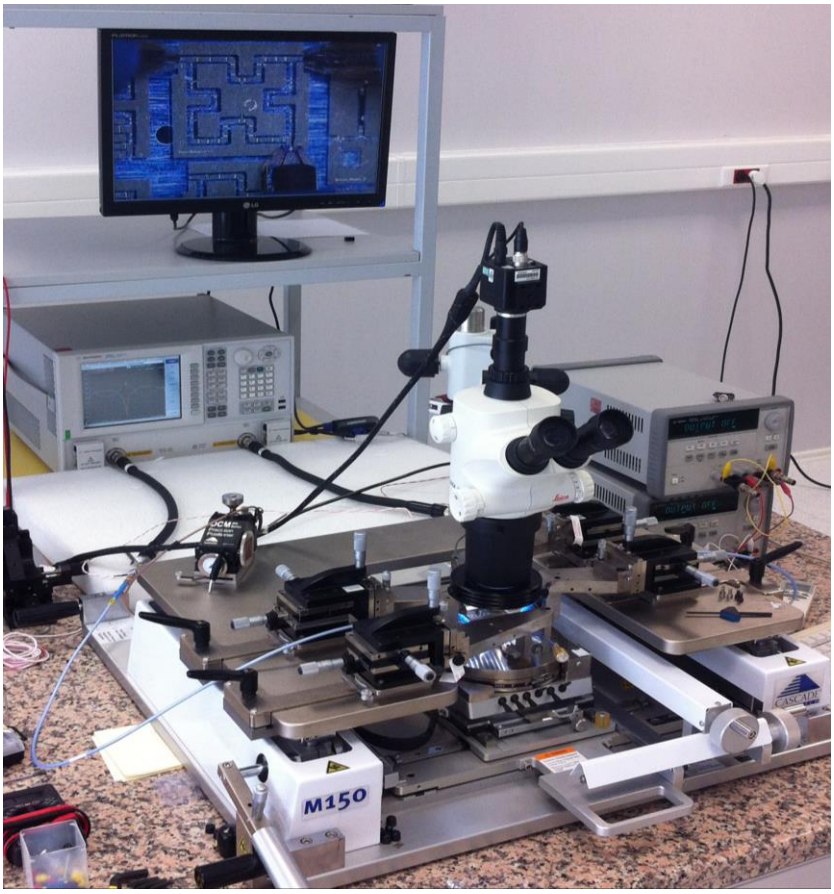

Figure 5.1: Photography of S-parameter Measurement Setup

In the S-parameter measurement, each port of the miniaturized branchline coupler (mBLC) was probed for on wafer measurements. In S-parameter measurements, the utilized power network analyzed (PNA) has the capability of having solely two (2) port measurements; because of this reason the third port of the mBLC was terminated with an external match load. In order to analyze the performances of the mBLCs, first coupled port of mBLC is terminated by match load and the first and second ports of the PNA were connected to the input and through ports of mBLC. After this measurement is finished, the through port of mBLC was terminated by match load, the first and second ports of the PNA were connected to the input and coupled ports of mBLC. Figure 5.2 illustrates the photography of on wafer S-parameter measurement.

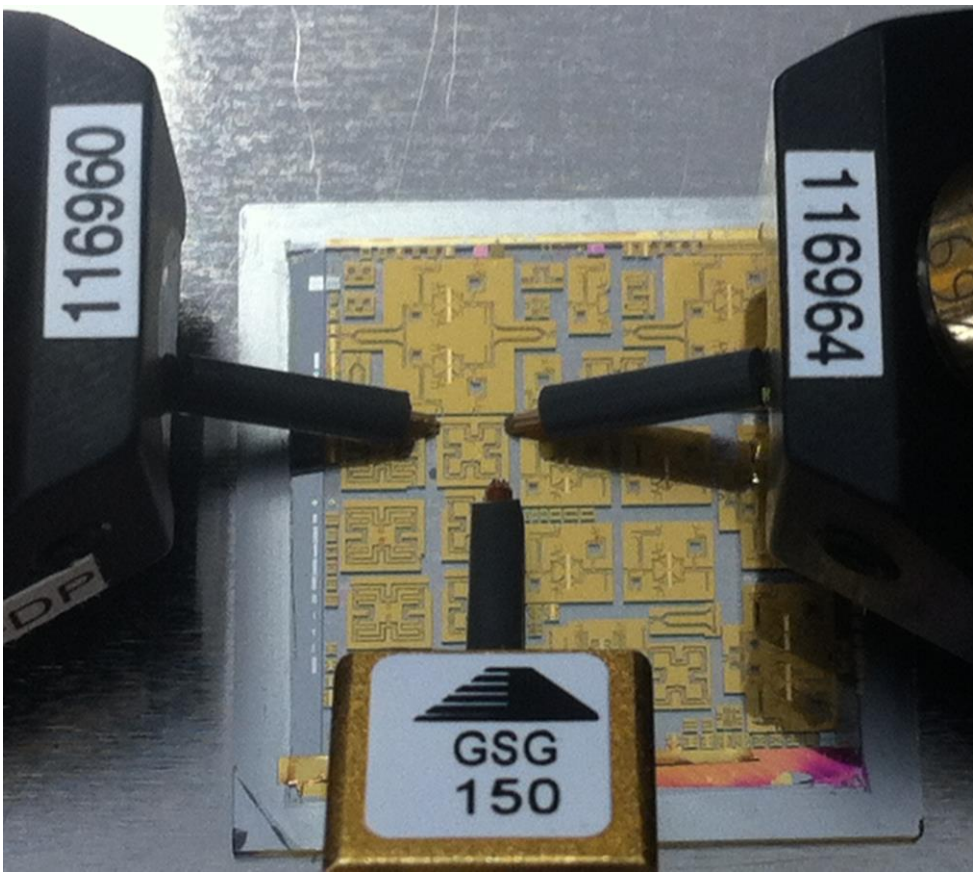

Figure 5.2: Photography of mBLC under test

5.1.1 S-Parameter Measurement Results of mBLC for the First Design

In the figure 5.3, the photography of the miniaturized branchline coupler (mBLC) for the first design is illustrated. The S-parameter measurement result of the mBLC for the first design was illustrated in the figure 5.4.

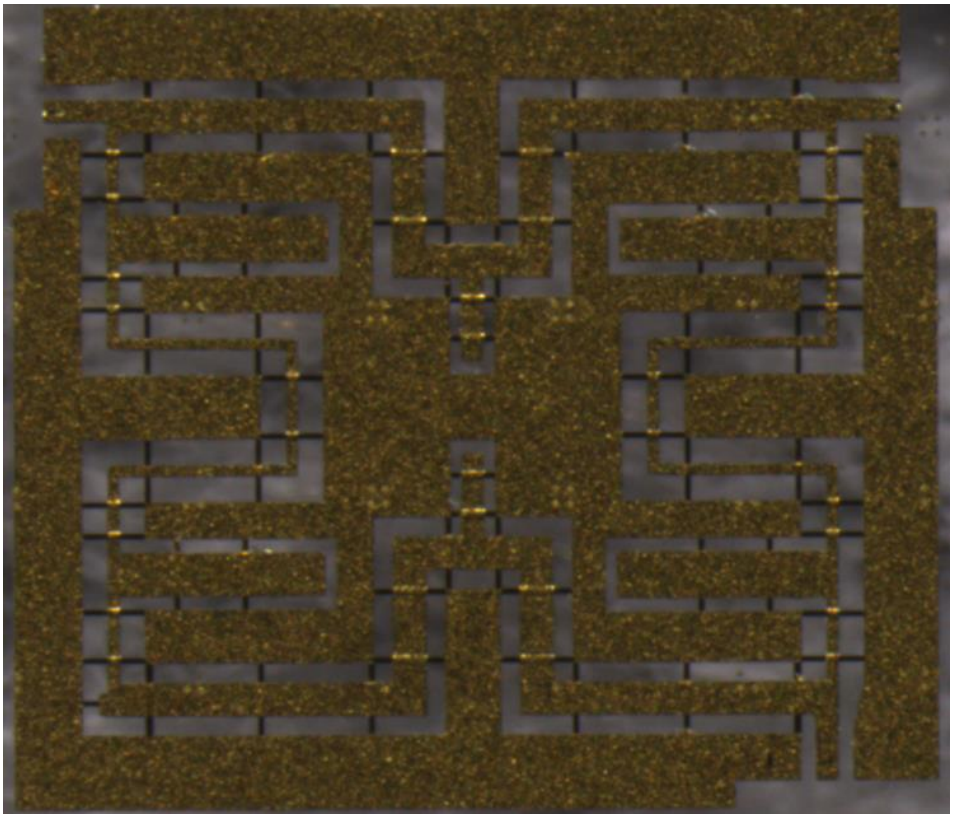

Figure 5.3: Photography of the first mBLC design

Figure 5.4 illustrates the s-parameter measurement results of the mBLC for the first design. To summarize S-parameter measurement results, the input and output reflections are better than -10dB over the frequency bandwidth of 8.4GHz to 11.1GHz. In additional to this, the through (S21) and coupling (S31) losses are approximately -3.5dB and -3.6dB at the center frequency. Moreover, the phase difference between the output ports are 90˚± 5˚ in the frequency range of 8.2 GHz to10.8GHz. The specs of the design is achieved in the frequency range of 8.4GHz to 10.8GHz with a 25% bandwidth.

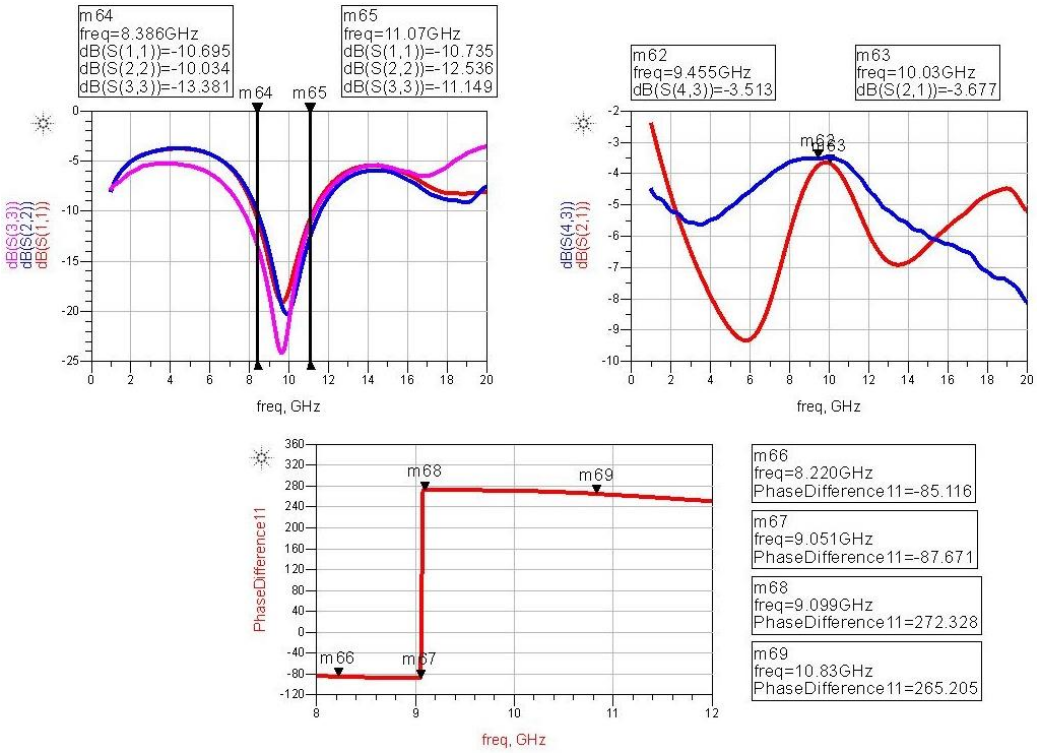

Figure 5.4: S-parameter Measurement Results of the first mBLC design

5.1.2 S-Parameter Measurement Results of mBLC for the Second Design

In the figure 5.5, the photography of the miniaturized branchline coupler (mBLC) for the second design is illustrated. The S-parameter measurement result of the mBLC for the second design was illustrated in the figure 5.6.

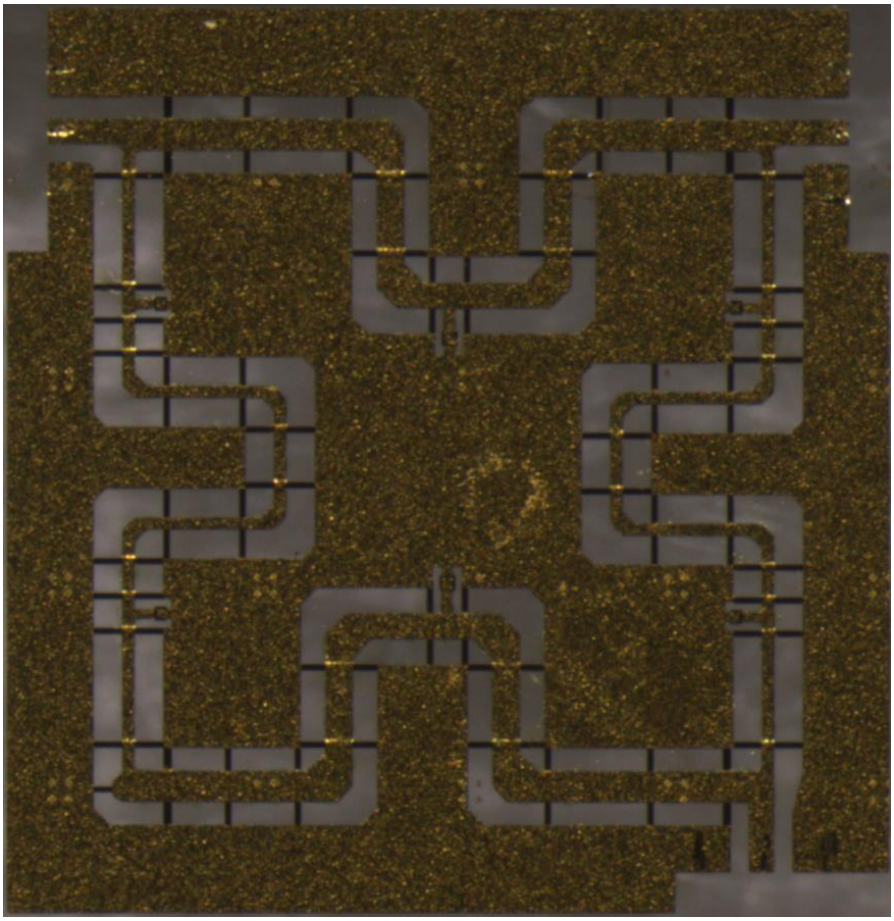

Figure 5.5: Photography of the second mBLC design

Figure 5.6 illustrates the s-parameter measurement results of the mBLC for the first design. According to the S-parameter measurement results, the input and output reflections are better than -10dB over the frequency bandwidth of 8.5GHz to 11.1GHz. In additional to this, the through (S21) and coupling (S31) losses are approximately -3.5dB and -3.6dB at the center frequency. Moreover, the phase

difference between the output ports are 90˚± 5˚ in the frequency range of 8.4 GHz to11.8GHz. The specs of the design is achieved in the frequency range of 8.5GHz to 11.1GHz with a 26.5% bandwidth.

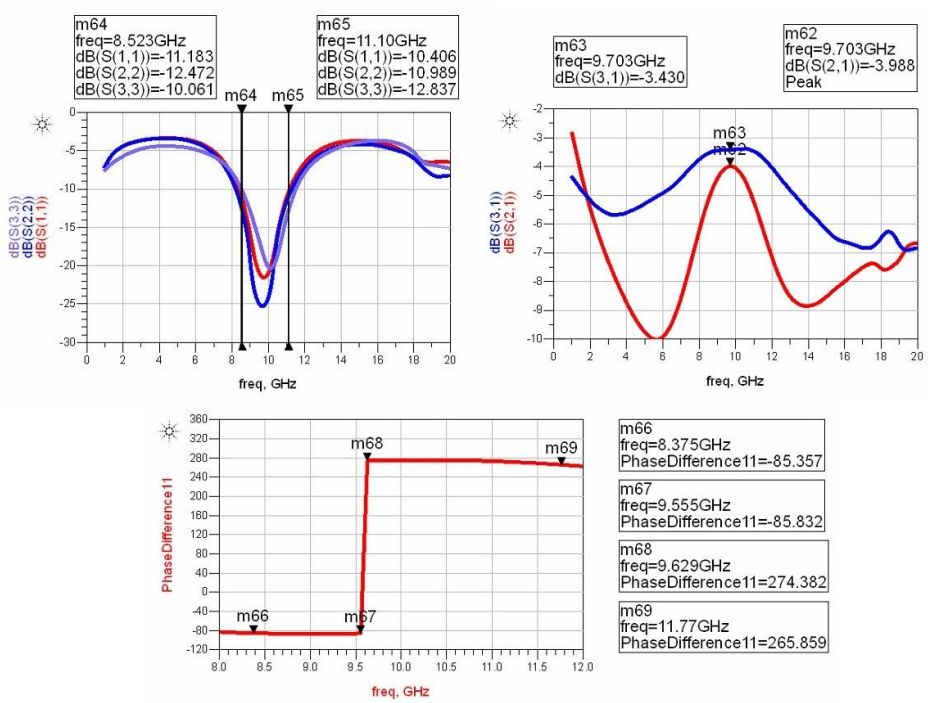

Figure 5.6: S-parameter Measurement Results of the second mBLC design

5.2 The Comparison of EM Simulation Results with Measurement Results

The electromagnetic simulations of the mBLC designs were done on both ADS Momentum 2.5D EM simulator and Sonnet Suites 3D EM simulators. In the EM simulation results, there were small differences in the through (S21) and coupled (S31) transmission. During the EM simulations, it was seen that if the mesh sizes were not sufficiently high, the difference between the simulation results of ADS Momentum and Sonnet Suites is more significant. In additional to this, if we increased the number of meshes sufficiently high, then the EM simulations results became similar and the differences between the results were ignorable.

5.2.1 The Comparison of EM Simulation Results with Measurement Results for the first mBLC design

Figures 5.7 and 5.8 illustrate the S-parameter and phase difference simulation results of ADS Momentum and Sonnet Suites, as well as the S-parameter measurement results of the fabricated mBLC for the first design.

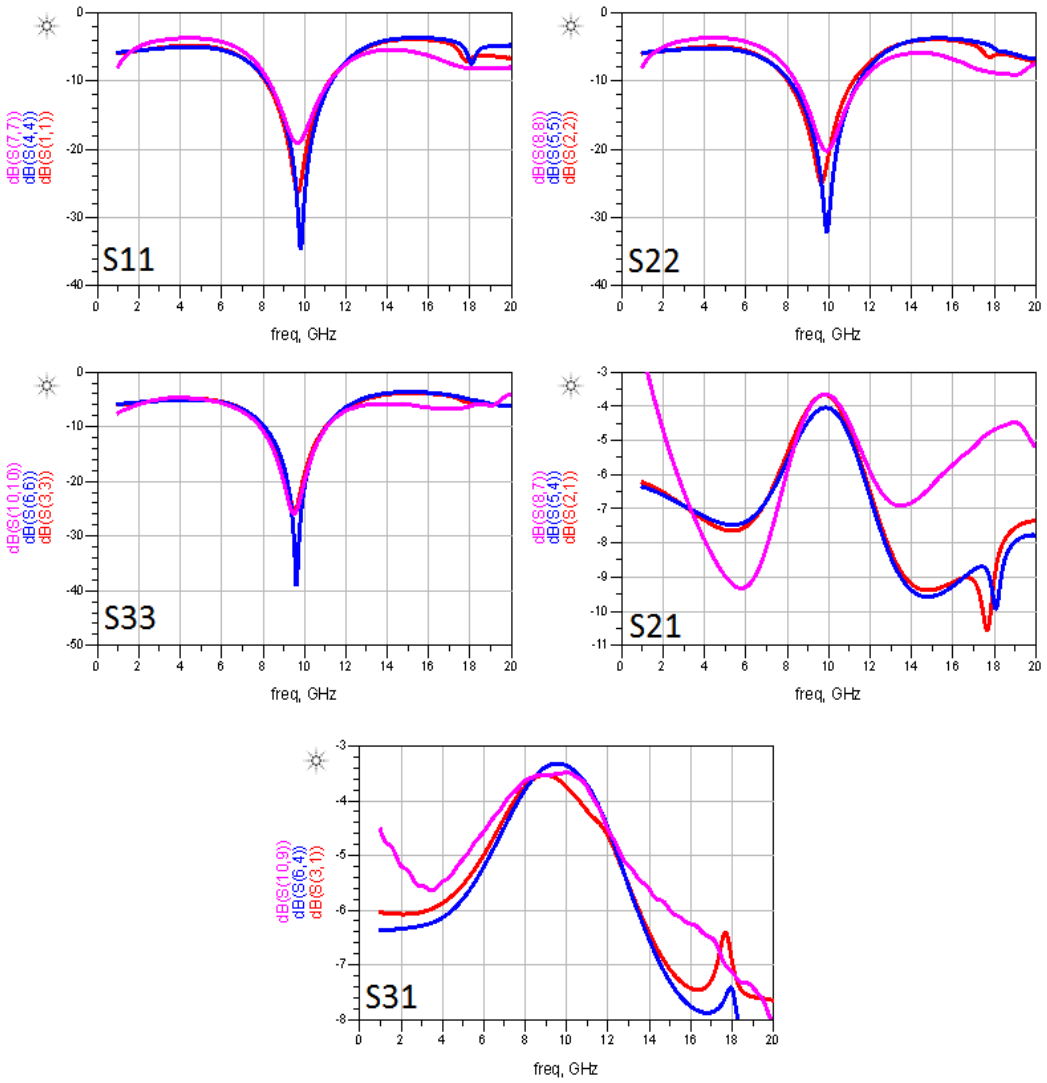

Figure 5.7: S-parameter Simulation and Measurement Results a) S11 b) S22 c) S33 d) S21 and e) S31 of the first mBLC design (EM Simulation Results of ADS Momentum (Red), EM Simulation Results of Sonnet Suietes (Blue) and Measured Results (Purple))

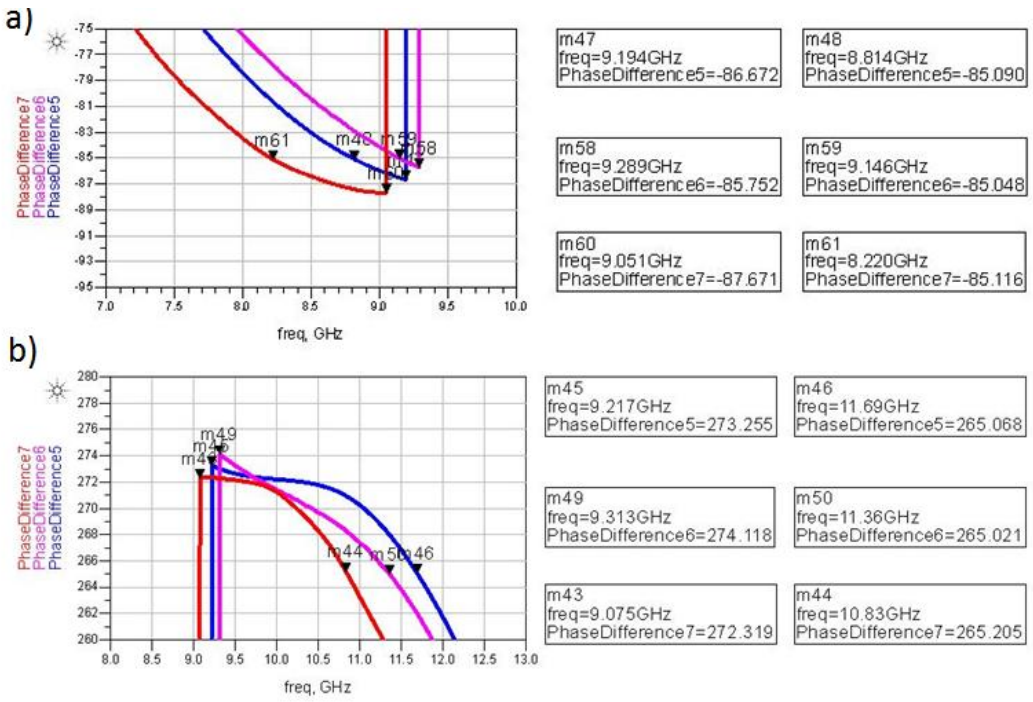

Figure 5.8: Phase Difference between the output ports of the first mBLC design in the frequency bandwidth of a) 7GHz - 10GHz b) 8GHz – 12 GHz (ADS Momentum (Red), Sonnet Suietes (Blue) and Measured Results (Purple))

Figures 5.7 and 5.8 show that S-parameter measurement results of the mBLC for the first design is in good agreement with the EM simulation results of ADS Momentum and Sonnet Suites. When we compare the measurement and simulation results, it is seen that there are small differences in the through and coupled port losses that can be caused by the metallization process of the fabrication and the conductivity of this layer seems to be worse than the parameters specified in simulators (in simulations the conductivity of this layer is taken as the conductivity of ideal gold). Although, there is slight difference in the losses of coupled and through port, according to S-parameter measurement, the operation frequency bandwidth of mBLC are in good agreement with the operation frequency bandwidth of the EM Simulation results.

In the table 5.1, the comparison of the EM simulations and measurement results of the first mBLC were done with reference to the center frequency and frequency bandwidth of the first mBLC measurement results.

Table 5.1: The Comparison of EM Simulation Results with Measurement Results of the first mBLC design

	ADS Momentum	**Sonnet Suites**	**Measurement Results**
S11 @ 8.4GHz	-12.5 dB	-14.5 dB	-10.7 dB
S11 @ 10.8GHz	-11.2 dB	-12.3 dB	-12.1 dB
S22 @ 8.4GHz	-13.5 dB	-15.3 dB	-10.4 dB
S22 @ 10.8GHz	-11.4 dB	-13.2 dB	-14.2 dB
S33 @ 8.4GHz	-13.9 dB	-15.3 dB	-13.9 dB
S33 @ 10.8GHz	-10.3 dB	-13.2 dB	-11.6 dB
S21 @ 9.6 GHz	-3.6 dB	-3.6 dB	-3.5 dB
S31 @ 9.6 GHz	-3.7 dB	-3.9 dB	-3.6 dB
Phase Difference @ 8.4GHz	83.6˚	82.8˚	86.2˚
Phase Difference @ 10.8GHz	270.1˚	263.7˚	265.4˚
EM Simulation Time Duration	1-2 Hours	5-6 Hours	-

5.2.2 The Comparison of EM Simulation Results with Measurement Results for the second mBLC design

Figures 5.9 and 5.10 illustrate the S-parameter and phase difference simulation results of ADS Momentum and Sonnet Suites, as well as the S-parameter measurement results of the fabricated mBLC for the second design.

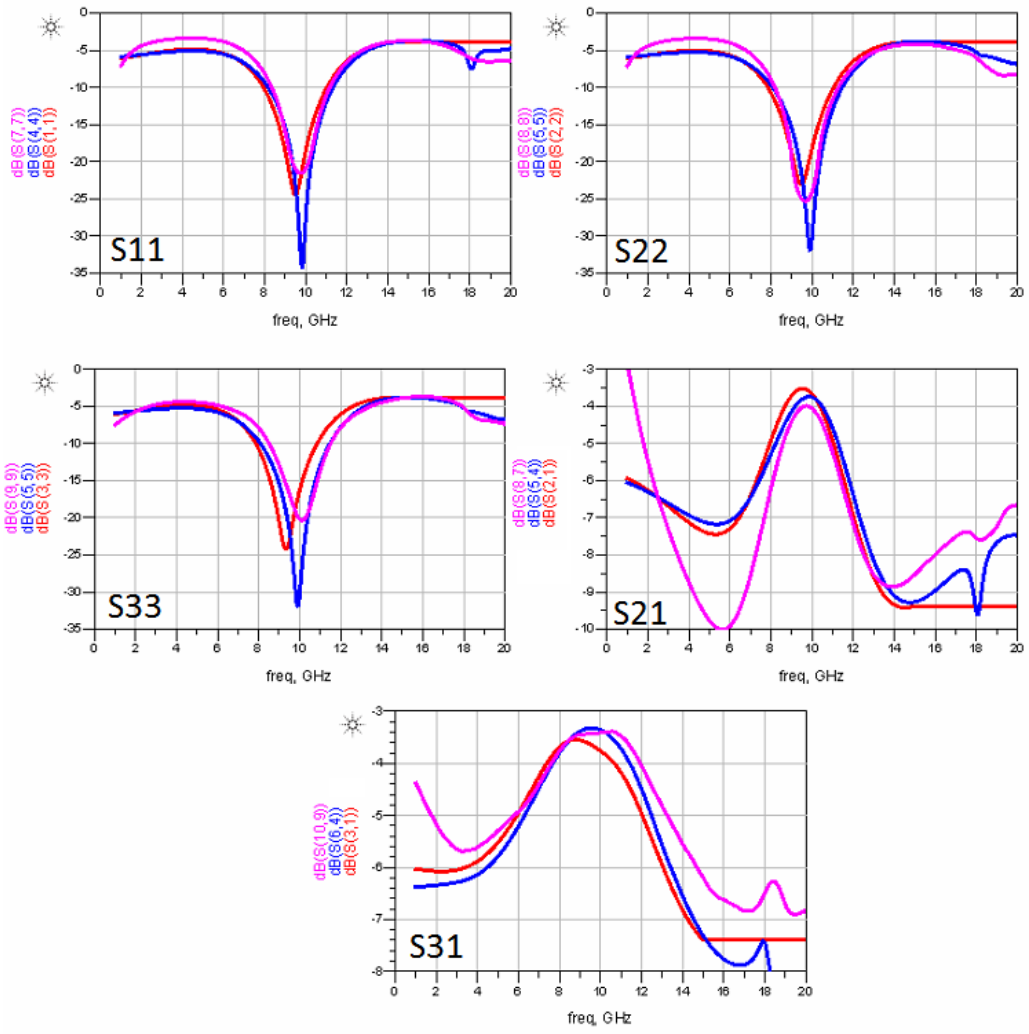

Figure 5.9: S-parameter Simulation and Measurement Results a) S11 b) S22 c) S33 d) S21 and e) S31 of the second mBLC design (EM Simulation Results of ADS Momentum (Red), EM Simulation Results of Sonnet Suietes (Blue) and Measured Results (Purple))

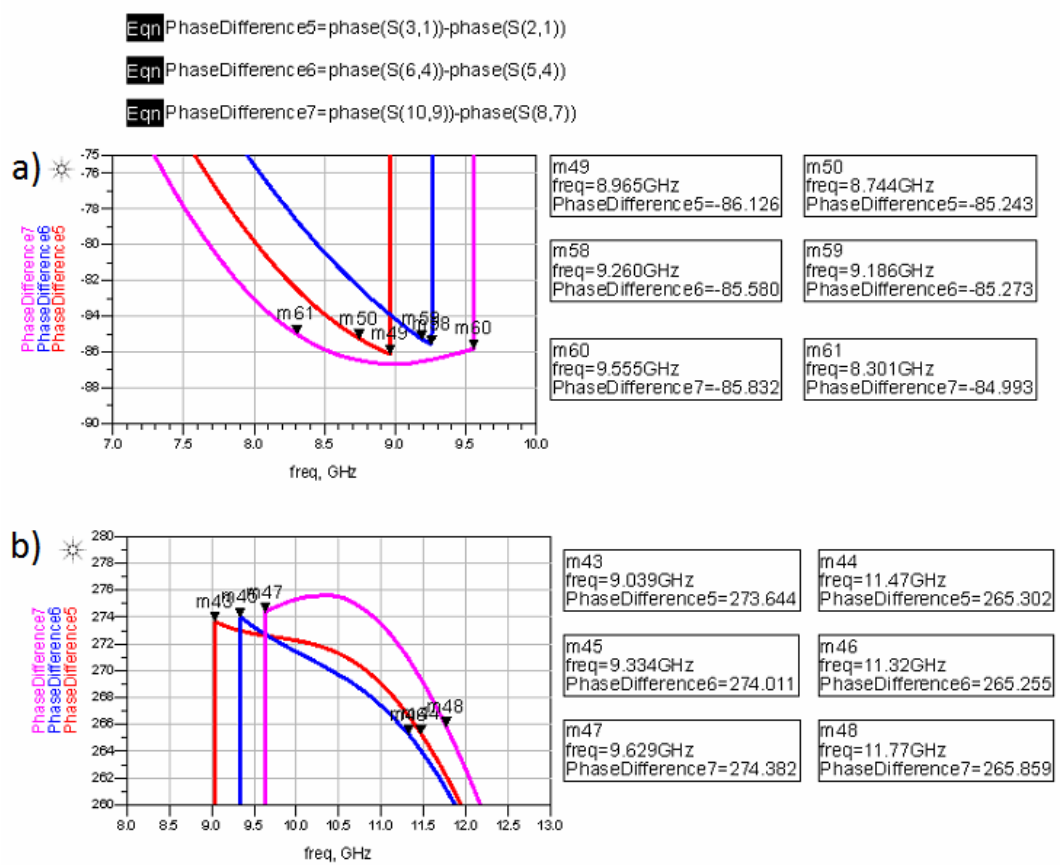

Figure 5.10: Phase Difference between the output ports of the second mBLC design in the frequency bandwidth of a) 7GHz - 10GHz b) 8GHz - 13 GHz (ADS Momentum (Red), Sonnet Suietes (Blue) and Measured Results (Purple))

Figures 5.9 and 5.10 show that the center frequency of the fabricated mBLC for the second design is approximately 500MHz shifted to the higher frequency, and the difference between the coupling and through losses are approximately 0.4dB at the center frequency. In this mBLC design, in the miniaturization techniques MIM capacitors were utilized. According to the test devices on the chip, the thickness of the Silicon Nitride passivation layer is larger than the design parameters. Due to this reason, the values of the MIM capacitors which were utilized in the miniaturization techniques are less than the designed values. Therefore, the center frequency of the mBLC design shifted to the higher frequency and the difference between the coupled and through port losses is increased.

In the table 5.2, the comparison of the EM simulations and measurement results of the second mBLC were done with reference to the center frequency and frequency bandwidth of the second mBLC measurement results.

Table 5. 2: The Comparison of EM Simulation Results with Measurement Results of the second mBLC design

	ADS Momentum	**Sonnet Suites**	**Measurement Results**
S11 @8.5GHz	-13.6 dB	-11.8 dB	-11.2 dB
S11 @11.1GHz	-9.6 dB	-11.3 dB	-10.4 dB
S22 @8.5GHz	-14.1 dB	-12.0 dB	-12.5 dB
S22 @11.1GHz	-10.5 dB	-13.3 dB	-11.9 dB
S22 @8.5GHz	-14.6 dB	-12.1 dB	-10.1 dB
S33 @11.1GHz	-8.9 dB	-12.2 dB	-12.8 dB
S21 @9.7GHz	-3.7 dB	-3.3 dB	-3.4 dB
S31 @9.7GHz	-3.5 dB	-3.7 dB	-4.0 dB
Phase Difference @8.5GHz	84.5 °	81.2 °	85.9 °
Phase Difference @11.1GHz	268.4 °	266.8 °	272.8°
EM Simulation Time Duration	1-2 Hours	5-6 Hours	-

CHAPTER 6

CONCLUSION & FUTURE WORKS

In this thesis work, it was aimed to design and characterize a miniaturized branchline coupler (mBLC) for the X-band monolithic microwave integrated circuit (MMIC) applications. The purposes of the design were significantly reducing the size of the branchline coupler with utilizing miniaturization techniques and widen the bandwidth of the operation. In the design of miniaturized branchline coupler (mBLC), first the theoretical analysis of the directional coupler was discussed. After that, branchline coupler, which is a special type of directional coupler, was theoretically analyzed and the properties of the BLC were described analytically. In additional to this, the miniaturization techniques were studied and their theoretical analyses of miniaturization techniques are investigated in detail. Following this, the design procedure of the mBLC is given step by step, simulation results are summarized for two different EM simulators, namely ADS Momentum and Sonnet Suites. Finally the measurement results or realized mBLCs are compared with the simulation results.

In order to design the miniaturized branchline coupler (mBLC), first of all, the ADS waveguide design tools were utilized and then the ideal elements were realized in the ADS Momentum. In additional to this, the electromagnetic (EM) simulations of the mBLC design were performed in the ADS Momentum 2.5D EM simulator. In the ADS Momentum, two different mBLCs were designed and simulated. In the design and simulations, since the final design will be fabricated using Bilkent University Nanotechnology Research Center's (NANOTAM) fabrication process, Bilkent University Nanotechnology Research Center's (NANOTAM) fabrication parameters were utilized. Moreover, 2D layouts of the designed and simulated mBLCs were

redrawn in the Sonnet Suites software and mBLCs were simulated in the 3D EM Sonnet Suite simulator and the results are compared with ADS Momentum. The details of the designed mBLCs and the simulation time comparison are given in the Table 6.1. Next, a photomask design was done for fabrication and designed mBLCs were fabricated.

Table 6.1: The Properties of Fabricated mBLCs

	First mBLC Design	**Second mBLC Design**
Sizes	1970um X 2320 um	1950um X 2000um
Sizes Reduction*	55%	62%
Bandwidth	25.0%	26.5%
Frequency Range	8.4 – 10.8GHz	8.5 – 11.1 GHz
Input/Output Return Loss	< -10 dB	< -10 dB
Phase Difference	90˚± 5 ˚	90˚± 5 ˚

*Reference to conventional BLCs

S-parameter measurements of the mBLCs were done. After that, S-parameter measurement results of the each mBLC design was compared with the EM simulation results of both ADS Momentum and Sonnet Suites.

In this thesis work, with using the miniaturization techniques, mBLCs with the chip dimensions of 2320x1970um (55% size reduction with respect to conventional BLC) and of 1950x2000um (62% size reduction with respect to conventional BLC) achieved in two different designs. Moreover, the frequency bandwidth of the first mBLC and second mBLC become 25% and 26.5% respectively. In the measurement step, it was seen that the EM simulation results of ADS Momentum and Sonnet

Suites are very similar to the S-parameter measurements. In additional to this, it was seen that 3D EM Sonnet simulator is more accurate than the 2.5D EM ADS Momentum simulator. However, the EM simulation time duration of Sonnet Suite is approximately 2-3 times longer than the EM simulation time duration of ADS Momentum. Therefore, there is a tradeoff between the accuracy and EM simulation time duration.

As a future work, the other types of miniaturization techniques can be applied and more reduction in the sizes of the mBLC design can be achieved. In additional to this, so as to utilize the mBLC designs in wideband applications, mBLCs with wider frequency response can be obtained. By this way, it would be possible to use mBLC in wideband MMIC power amplifier applications.

REFERENCES

[1] Cohn, S.B., Levy, R., "History of Microwave Passive Components with Particular Attention to Directional Couplers", IEEE Transaction Microwave Theory and Techniques, vol.32, no.9, September 1984.

[2] Rodrigues, S., Fajardo, A., Paez, C., "Characterization of the Branch-line and Rat-Race ideal Hybrids through Their Merit Parameters", Second Latin American Symposium Circuits and Systems (LASCAS), 2011 IEEE.

[3] Young, H.C., Jia, S.H., "Design of a Compact Broadband Branch-Line Hybrid", Microwave Symposium Digest 2005, IEEE MTT-S International.

[4] Yi, C.C., Chong, Y.C., "Design of a Wide-Band Lumped-Element 3-dB Quadrature Coupler", IEEE Transaction on Microwave Theory and Techniques, vol.49, no.3, March 2001.

[5] Sakagami, I., Tuya, W., "Impedance-Transforming Lumped-Element Co-directional Couplers and Their Circuit Structure", APMC 2005 Proceedings, IEEE.

[6] Toker, C., Saglam, M., Ozme, M., Gunalp, N., "Branch-Line Couplers Using Unequal Line Lengths", IEEE Transactions on Microwave Theory and Techniques, vol.49, no.4, April 2001.

[7] D.M. Pozar, "Microwave Engineering", 3rd Edition, New York, J. Willey, 2005.

[8] https://www.sonnetsoftware.com/products/sonnet-suites/, last accessed on 06/06/2014

[9] L. Piazzon, “The Doherty amplifier and beyond theoretical analysis and design guidelines about the Doherty power amplifier and its evolution”, Doctorate Thesis, 2010.

[10] http://www.home.agilent.com/upload/cmc_upload/All/Gustrau_FHDortmund_EMDSforADS.pdf?&cc=TR&lc=eng, last accessed on 26/06/2014

[11] Maloratsky L. G., “Passive RF & Microwave Integrated Circuit”, Elsevier, 2004.

[12] Kimberley, W., Sebastian, H.M., “Compact Planar Microstripline Branch-Line and Rat-Race Couplers”, IEEE Transaction on Microwave Theory and Techniques, vol.51, no.10, October 2003.

[13] Bowick, C., Blyler, J. and Ajluni, C., “RF Circuit Design”, 2nd Edition, Elsevier Science & Technology, 2007.

[14] Ulaby, F.T., Michilssen, E. and Ravaioli, U., “Fundamentals of Applied Electromagnetics”, 6th Edition, Prentice Hall, 2010.

[15] Reed, J. and Wheeler, G. J., "A Method of Analysis of Symmetrical Four-Port Networks", Microwave Theory and Techniques, IRE Transactions on, vol.4, no.4, 1956, pp.246-252.

[16] Toker, C., “METU EE527 Microwave Engineering Lecture Notes”, 2012

[17] http://www.wisegeek.com/what-is-a-photomask.htm, last accessed on 30/06/2014

[18] Li, B., Wu, X., Wu, W., " A Miniaturized Branch-Line Coupler with Wideband Harmonic Suppression", Progress in Electromagnetic Research Letters, vol.12, 2010, pp.181-189.

[19] Hirota, T., Minakawa, A., Muraguchi, M., "Reduced-Size Branch-line and Rat-Race Hybrids for Uniplanar MMIC's", IEEE Transaction on Microwave Theory and Techniques", vol.38, no.3, 1990.

[20] Cheng, K.M., Wong, F.L., "A Novel Approach to the Design and Implementation of Dual-Band Compact Planar 90 Branch-Line Coupler", IEEE Transaction on Microwave Theory and Techniques", vol.52, no.11, 2004.

[21] Ghali, H., Moselhy, T., "Miniaturized Fractal Rat-Race, Branch-Line, and Coupled-Line Hybrids", IEEE Transaction on Microwave Theory and Techniques", vol.52, no.11, 2004.

[22] Dasgupta, D., Sarkar, B., Pal, M., Ghatak, R., "Miniaturized planar branch-line coupler with asymmetrical π-shaped structure", National Congress on Communication, 2013.

[23] Haroun, I., "A Compact 81-86 GHz Branch Line Coupler using End-Loaded Transmission Lines", Radio and Wireless Symposium (RWS), 2012 IEEE.